sciendo
Austrian Journal of Earth Sciences | Vienna | 2018 | Volume 111/2 | 180 - 203 | DOI: 10.17738/ajes.2018.00012

Early late-glacial rock avalanche and its lasting effects on drainage and sediment dispersal (Strassberg valley catchment, Northern Calcareous Alps, Austria)

Diethard SANDERS[1) *)], Hannah POMELLA[1)] & Charlotte GILD[2)]
[1)] Institute of Geology, University of Innsbruck, A-6020 Innsbruck, Austria;
[2)] Institute of Geography, University of Innsbruck, A-6020 Innsbruck, Austria;
[*)] Corresponding author: Diethard.G.Sanders@uibk.ac.at

KEYWORDS Alps; landslide; Quaternary; paraglacial; catchment; canyon

Abstract

In intramontane landscapes shaped by glacial-interglacial cycles, the most rapid changes during the proglacial/paraglacial phases may be amplified by catastrophic mass-wasting. Herein, we describe the Last Glacial Maximum (LGM) to Holocene development of a catchment in the Northern Calcareous Alps wherein intense proglacial/paraglacial sedimentation and descend of a rock avalanche persistently modified drainage and sediment dispersal.

During buildup of the LGM, the pre-last glacial Strassberg valley – the trunk valley of this study – was filled with a proglacial fluvio-lacustrine succession. Thereafter, the area became largely buried under the Inn ice stream. During deglacial ice melt, copious sediment was shed from glacially-conditioned mountain flanks. Alluvial fans cut off from their former supply area, and perched in isolated position, result from presumed sediment dispersal across dead ice. Shortly after deglaciation, a ~11 Mm^3 rock avalanche detached from a high cliff, overran an opposing mountain ridge, and spread over a lower-positioned plateau. The rock avalanche blocked the Strassberg valley and set the base-level to an intramontane basin that persists until present. A quartz OSL age from a loess drape above the rock-avalanche deposit dates mass wasting prior to 18.77 ± 1.55 ka; so far, this is the oldest age-bracketed post-LGM catastrophic mass-wasting of the Eastern Alps.

After mass wasting, the valley was barred by the rock-avalanche deposit. This, in turn, triggered a westward switch of drainage thalweg and stream incision. The present Strassberg valley is an epigenetic bedrock gorge 1.5 km in length and down to 100 m in depth. A $^{234}U/^{230}Th$ calcite disequilibrium age of 9 ± 1 ka from cemented talus indicates that most incision took place during the late-glacial to early Holocene. Aside of the large-scale morphology (valleys, ranges) the drainage, the smaller-scale morphology, and the sediment volumes of the study area are mainly coined by proglacial/paraglacial processes and by rock avalanching. Holocene landscape changes are modest and chiefly comprise aggradation of high-positioned scree slopes, colluvial/alluvial redeposition and stream incision, and slope stabilization by reforestation. Our results underscore that intramontane sceneries are mosaics with respect to the age of landforms and that large parts of the landscape still are off geomorphic equilibrium with interglacial conditions.

1. Introduction

Aside of large-scale long-term relief development, intramontane landscapes may undergo switches in configuration caused, either, by climatically-steered changes in sediment availability and dispersal, and/or by stochastic events such as catastrophic mass wasting. In mountain ranges undergoing glacial-interglacial cycles, the most significant changes of sedimentation regime take place (i) during climatic cooling and glacial advance, and (ii) during to shortly after deglaciation. In the Eastern Alps, thick successions of glacio-fluvial/lacustrine deposits accumulated under cold climates during advance of valley glaciers or ice streams (e.g., Penck and Brückner, 1909; Van Husen, 1983; Ostermann et al., 2006; Sanders et al., 2014; Barrett et al., 2017). Deglacial-paraglacial landscape changes, in contrast, are mainly related to: (a) development of short-lived deposystems (e.g., ice-marginal lakes, kames), (b) rapid sedimentation in proximal-alluvial and slope deposystems, and (c) re-incision of streams and partial re-organization of drainage (e.g., Reitner, 2007; Sanders et al., 2009; Sanders and Ostermann, 2011; Sanders, 2012; Sanders et al., 2014).

Extremely-rapid or 'catastrophic' mass-wastings (CMWs) of rock >10^5 m^3 in volume (rockslides, rock avalanches; Evans et al., 2006), in contrast, take place independently of glacial retreat. Compiled numerical ages of CMWs show that up to >10 ka may pass from deglaciation to large-scale slope failure (Prager et al., 2008; Ostermann et al., 2016). A clear-cut association of CMWs with seismogenic fault zones implies that rock disintegration and deformation are most relevant to prepare slopes for failure and, via macroseismic events, to trigger CMW detachment (Lenhardt, 2007; Prager et al., 2008; Ostermann and Sanders, 2016). In many cases, CMWs impart changes of landscape development mainly by transient or long-term blockade of valleys (cf. Hewitt, 1998; Korup and Tweed, 2007; Prager et al., 2008; von Poschinger and Kippel, 2009; Schneider et al., 2011). In the Alps, at least 600 CMWs mostly younger than the Last Glacial Maximum (LGM) are

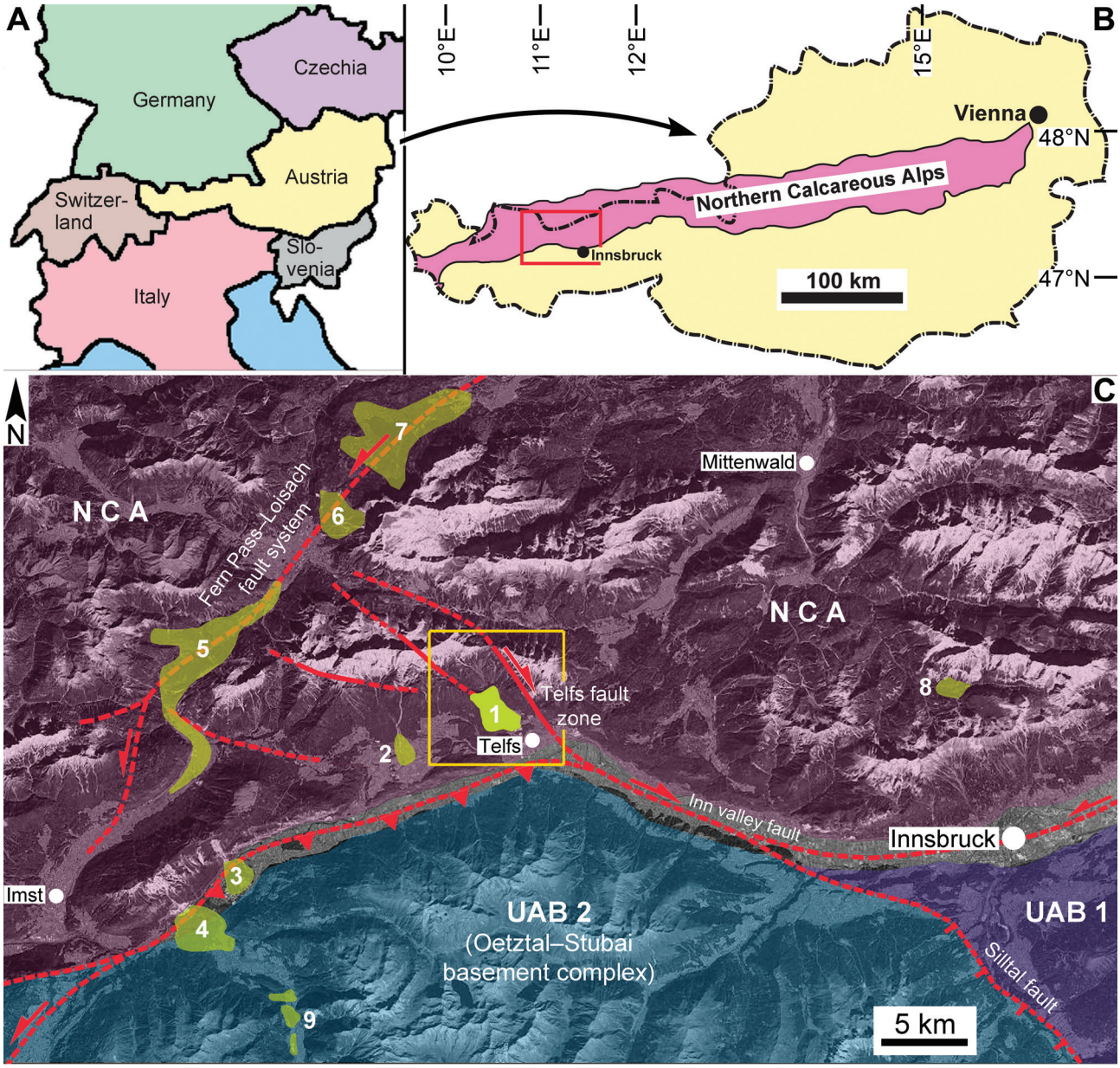

UAB 1, UAB 2: Upper Austroalpine basement; NCA: Northern Calcareous Alps
1: Strassberg (this paper); 2: Stöttlbach; 3: Haiming; 4: Tschirgant; 5: Fern Pass;
6: Grainau; 7: Eibsee; 8: Birchegg; 9: Habichen–Tumpen–Burgstein

Figure 1: (A) Position of Austria in Europe. (B) Northern Calcareous Alps, with area of subfigure C indicated. (C) Environs of study area, showing major structural units, faults, and catastrophic mass-wastings of rock (labeled 1 to 9). The yellow rectangle marks the area shown in Fig. 2. Background satellite image from Bingmaps® (download on 10.5.2016).

identified so far (Ostermann and Sanders, 2012). Aside of proglacial/paraglacial processes, mass-wasting thus may also exert lasting effects on morphology, drainage and sedimentation.

In the present paper, a catchment in the Northern Calcareous Alps (NCA) is described that was shaped by superposition of proglacial and deglacial–paraglacial processes as well as by rock avalanching (Fig. 1). The rock avalanche deposit – described herein for the first time in detail (Fig. 2) – is the oldest age-dated post-LGM catastrophic mass-wasting identified so far in the Eastern Alps. Rock avalanching triggered the formation of an intramontane basin and incision of an epigenetic bedrock gorge. Together, the proglacial/paraglacial processes and rock avalanching exerted a significant and lasting imprint on landscape development.

2. Methods

The study area was mapped in the field on isohypsed laserscan terrain models. The altitude above sea level of outcrops is based on a 1-m digital elevation model provided free by the Tyrolian federal government (http://portal.tirol.gv.at/weboffice/tirisMaps). For a mass-wasting to classify as extremely rapid, a peak propagation velocity >5 m/s is required (Hungr et al., 2001); if an extremely rapid mass-wasting involves a rock volume ≥ 10^5 cbm

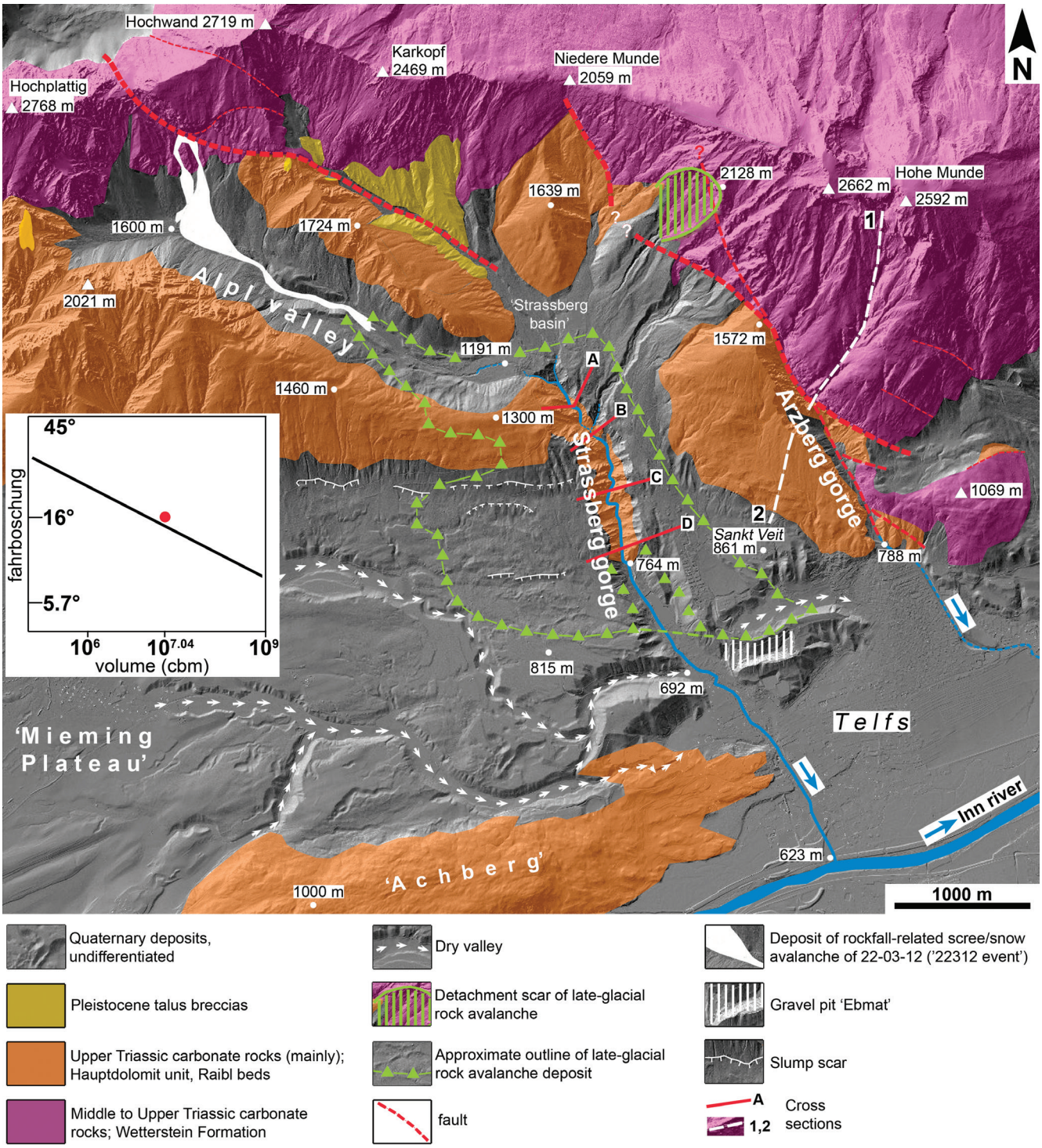

Figure 2: Map of study area. The major fault planes (Telfs fault system, cf. Fig. 1) dip subvertical. Inset diagram shows correlation of fahrboschung with rock volume for 11-Mm^3 rock avalanche deposit described herein; black line (from Collins and Melosh, 2003, their Fig. 1) is the linear regression for a large number of catastrophic mass-wastings. See text for further description.

(Evans et al., 2006), the term 'catastrophic' may be applied (e.g., Sanders et al., 2010; Ostermann and Sanders, 2016). This does not exclude lower velocities during the terminal phase of runout (cf. Crosta et al., 2004). During descend, rock avalanches disintegrate into numerous blocks and typically spread out as sheet-like sediment bodies (Evans et al., 2006). The volume of the detachment scar of the rock avalanche was calculated using ESRI ArcGIS Desktop 10.5 facilities. Digital Elevation Model data (© Land Tirol) used to quantify the volume of the detachment scar are provided free by the Federal State of Tyrol to certified users of the University of Innsbruck. We approximated the former cliff surface and calculated the differential volume between the cliff surface and the LIDAR digital elevation model. In order to make a valid reconstruction of the former cliff surface we used several surface analysis

tools (part of the extension "Spatial Analyst") to analyse the shape and orientation of the slopes surrounding the detachment scar: the "Slope" tool identifies the steepness at each cell of a raster surface, the "Curvature" tool calculates the curvature of a raster surface, and the "Aspect" tool identifies the compass direction that the downhill slope faces for each location. In the next step, the former cliff surface was approximated by constructing contour lines fitting the characteristic geometries of the surrounding slopes. These contour lines where used to interpolate the former surface using the "Topo to raster" tool, which interpolates a hydrologically correct raster surface. Finally, the reconstructed surface and the LIDAR digital elevation model where analysed with the "Cut Fill" tool (Extension "3D Analyst", calculating the volume change between the two surfaces. In order to assess the changes in calculated volume based on different slope reconstructions, several slightly different former cliff surfaces have been modelled; the difference was within a few percent. No comparison was made between the volume of the rock avalanche as deduced from the detachment scar and the volume of the rock-avalanche deposit. The reason for this is that – as suggested from outcrops (see below) – the thickness of the rock-avalanche deposit (RAD) is highly variable which renders a meaningful volume calculation of the deposit hardly possible.

For radiocarbon dating of soils that overlie the RAD, the sieved and acid-washed bulk organic fraction was used. In this procedure, the soil first is sieved to < 180 microns to sort out particles (e.g., rootlets, fragments of arthropod carapaci), followed by acid washing to remove carbonate minerals. This treatment cannot identify younger humic acids that post-date the first formation of a soil level; if younger humic acids are admixed, radiocarbon ages tend to be younger than the depositional age (Geyh, 2005; cf. Sanders et al., 2018). To minimize the younging bias, soil samples from different levels and locations were taken. In an open construction pit, a layer of polymictic siliciclastic silt (loess) was found to directly overlie the RAD. This loess layer is part of a widespread veneer of late-glacial loess identified in the NCA including the study area (Niederstrasser, 2017; Gild et al., 2018). The layer was sampled for optically-stimulated luminescence (OSL) dating of quartz. The sample was processed in the Laboratory of Luminescence Dating of the University of Oxford (Lab identfication number L01/22).

3. Terms and definitions

For clasts up to cobble size, the Udden-Wentworth scale of grain-size classification was used. Further, we designate clasts of 0.256 m to 10 m in diameter as boulders; larger clasts between 10-100 m in size are termed mesoliths (cf. Sundell and Fisher, 1985; Heck and Speed, 1987). The terminology of stream channel types follows Montgomery and Buffington (1997). To date, there exists no formalized classification of clastic sediments produced by fragmentation within rockslides and rock avalanches. Pollet and Schneider (2004) used the terms cataclasis (process), and cataclastic horizons and gouge (unlithified rock powder produced by cataclasis) for their description of the Flims CMW. Before the issue of classification is settled, we follow their use of terms, albeit it is not strictly concordant with the use in structural geology.

The term paraglacial was introduced by Church and Ryder (1972, p. 3059) for "nonglacial processes that are directly conditioned by glaciation. It refers both to proglacial processes, and to those occurring around and within the margins of a former glacier that are the direct result of the earlier presence of the ice." The term initially was used mainly for the reworking of glacigenic sediments immediately after glacier retreat (e.g., Ballantyne and Benn, 1994; Curry and Ballantyne, 1999, p. 409; Benn and Owen, 2002; Curry et al., 2006; Meigs et al., 2006). Ballantyne (2002) widened the scope of the term to include all processes related to former glaciation, even if these were manifest thousands of years thereafter, such as mass wastings (e.g., Cossart et al., 2008; Kellerer-Pirklbauer et al., 2010; Ballantyne and Stone, 2013; Ballantyne et al., 2014). Furthermore, a clear-cut end of paraglacial sediment dispersal can hardly be set because it is a gradual fadeout in space and time that, too, may last over thousands of years (cf., André, 2003; Orwin & Smart 2004; Schrott et al., 2004; Sanders and Ostermann, 2011; Tunnicliffe and Church 2011). In some cases, a 'primary' paraglacial activity was distinguished from a subsequent 'secondary' paraglacial activity (Ballantyne, 2002; Ravazzi et al., 2012). An even wider understanding of paraglacial was presented by French and Harbor (2013, p. 3) who designated it as "the disequilibrium that occurs as one geomorphic environment moves from one equilibrium condition to another." As the understanding of the term evolved, today it comprises processes related to former glaciation, and that may be active over thousands of years. In some cases, however, in particular with respect to the collapse of pleniglacial ice streams and its consequences, it is desirable to distinguish between (i) the phase of ice decay *sensu stricto* (= deglacial phase, or deglacial) and (ii) processes related to glaciation, but that extend over a longer time span than the former phase, and that may be of waning intensity and extent in space and time (= paraglacial phase, or paraglacial) (Gild et al., 2018; cf. Ravazzi et al., 2012).

4. Setting

4.1 Rock substrate

The study area is located near the southern margin of the NCA (part of the Eastern Alps), a nappe edifice dominated by Triassic shallow-water carbonate rocks (Fig. 1) (Tollmann, 1976; Mandl, 1999). The succession of the NCA accumulated on a rifted passive margin that was telescoped into stacked thrust nappes (e.g., Ratschbacher et al., 1991; Schmid et al., 2004; Handy et al., 2015). Since the latest Eocene, the nappe stack of the Eastern Alps became indented by a northward-pushing crustal segment ('Dolomites indenter', Frisch et al., 2000) of the Southern Alps. Tectonic indentation dismembered the nappe edifice

Name, age range	Lithologies, remarks	Interpretation, references
Wetterstein Limestone; Middle to Upper Triassic (Ladinian to Carnian *pro parte*)	Very-thick bedded, light grey limestones Intercalated strata of loferites and cryptmicrobially-laminated limestones Local domains of beige coloured, coarse crystalline epigenetic dolostones	Limestones, locally dolomitized, of shallow neritic to peritidal carbonate environments
Northern Alpine Raibl beds; Upper Triassic (Carnian *pro parte*)	Typical: (1) Oncolite beds (2) marly bioclastic limestones (3) black silty slates (4) cellular dolomites with relicts of sulfate evaporites	Mixed siliciclastic-carbonate-evaporite succession of neritic to peritidal environments
Hauptdolomit unit; Upper Triassic (Norian *pro parte*)	(1) Brownish to grey weathered, medium- to thick-bedded (sucrosic) dolostones (2) layers of loferitic dolostones and cryptmicrobially-laminated dolomicrites (3) mm- to cm-rhythmites of dolomicrite	Deposition of early-dolomitized limestone in the peritidal environment of a large carbonate platform

Table 1: Stratigraphic units of rock substrate in the study area.

along large strike-slip faults (e.g., Inn valley fault; Fig. 1), and led to uplift of metamorphic core complexes bounded by detachments and normal fault zones (Fig. 1) (e.g., Linzer et al., 1995, 1997; Fügenschuh et al., 1997, 2012; Wang and Neubauer, 1998; Ortner et al., 2006; Wölfler et al., 2011). High seismic activity along the fault zones and remote sensing indicate that indentation and uplift persists, or is reactivated (e.g., Reinecker and Lenhardt, 1999; Reiter et al., 2005; Lenhardt et al., 2007; Caporali et al., 2013; Nasir et al., 2013; Reiter, 2017). In the study area, the 'Telfs system' of dextral strike-slip faults developed in reaction to NW-ward thrusting of the Oetztal-Stubai basement block adjacent to the South (Figs. 1 and 2) (Linzer et al., 2002; Reiter et al., 2005). Faulting still is active, as indicated by numerous historical and instrumental records of earthquakes of magnitudes up to > 6 (Reinecker and Lenhardt, 1999; Reiter, 2017). Another component of indentation-related deformation is relayed via sinistral faults – such as the Fern Pass-Loisach fault (Fig. 1) and associated catastrophic mass-wastings – to the northern margin of the NCA (Linzer et al., 2002; Ostermann and Sanders, 2016).

The study area comprises three stratigraphic units (Fig. 2; Table 1). Of these, the Wetterstein Limestone supports the highest summits and cliffs (Fig. 2). The Northern Alpine Raibl beds, in contrast, weather back and are mostly covered. Lower crests and rounded ridges in the southern part of the study area consist of the dolostone succession of the Hauptdolomit unit (Fig. 2). During Alpine deformation, these dolostones reacted brittlely and became densely jointed and faulted, resulting in high erodability; this contributed to formation of a plateau-like widening ('Mieming Plateau') along the Inn valley (Fig. 2). The Mieming Plateau is veneered by Quaternary sediments, but an overall plateau shape is also excavated from the underlying bedrock (Herbst et al., 2009). This is supported by the gently sloping intersection of the bedrock brinkline of Strassberg gorge with the till-veneered plateau surface (Figs. 2, 3).

4.2 Quaternary

4.2.1 Last Glacial Maximum

The main Quaternary deposits of the study area are summarized in Table 2. In the Eastern Alps, four full glaciations are identified, but phases of significant advance of valley glaciers also are recorded (see Van Husen and Reitner, 2011; Reitner et al., 2016; Barrett et al., 2017). In the considered area, proglacial outwash and till are rich in clasts of metamorphic rocks from the catchment of the Inn ice stream (Ampferer, 1904; Penck and Brückner, 1909; Machatschek, 1934; Mutschlechner, 1948).

The local succession of the LGM consists of (i) proglacial fluvio-lacustrine deposits overlain by (ii) basal till of the Inn ice stream (Fig. 3, Table 2). The till typically is a matrix-supported diamicton with pebbles of metamorphic rocks and carbonate rocks. Near the SW margin of the study area, drillings revealed that the proglacial to glacial succession is at least 140 m in thickness, and (b) that the LGM till is based by an unconformable surface with a vertical relief of tens of meters (Herbst et al., 2009). Together, the proglacial succession and the basal till cover an older bedrock relief (Fig. 3). In the proglacial succession, in gravel pit 'Ebmat', a package ~70 m in thickness of pebbly fan-delta foresets is present (Figs. 2, 3) (Poscher, 1993) that dip to SE-SSW; the foresets consist of pebbles from the NCA and ≤10% of pebbles of metamorphic rocks. The proglacial fan delta was not supplied from the presently active bedrock canyon, but from a pre-LGM 'precursor Strassberg valley' (Poscher, 1993) that is clogged until today with deposits of the LGM and of a rock avalanche (Fig. 3) (see below for details). During the LGM, the summit of Hohe Munde (2662 m) and the range from Karkopf (2469 m) to Hochplattig (2768 m) were nunataks above an upper ice margin of ~2200-2100 m a.s.l. (cf. Fig. 2) (cf. Mutschlechner, 1949; Van Husen, 1987). Limited transfluence of the Inn ice stream across the southern crest of Alpl valley is indicated by a few clasts of metamorphic rocks up to 1600 m a.s.l. near the valley head (Fig. 2).

4.2.2 Deglacial to late-glacial interval

The interval of post-LGM climatic warming that was punctuated by stadials, i.e., by episodes of cooling and glacial re-advance, is termed the late-glacial (Penck and Brückner, 1909; Reitner, 2007; Auer et al., 2014; Reitner et al., 2016). The late-glacial started between ~20-19 ka, when the ice streams stagnated and decayed, and lasted up to 11.7 ka BP (beginning of the Holocene, Severinghaus et al., 1998; cf. Auer et al., 2014). Along Alpl

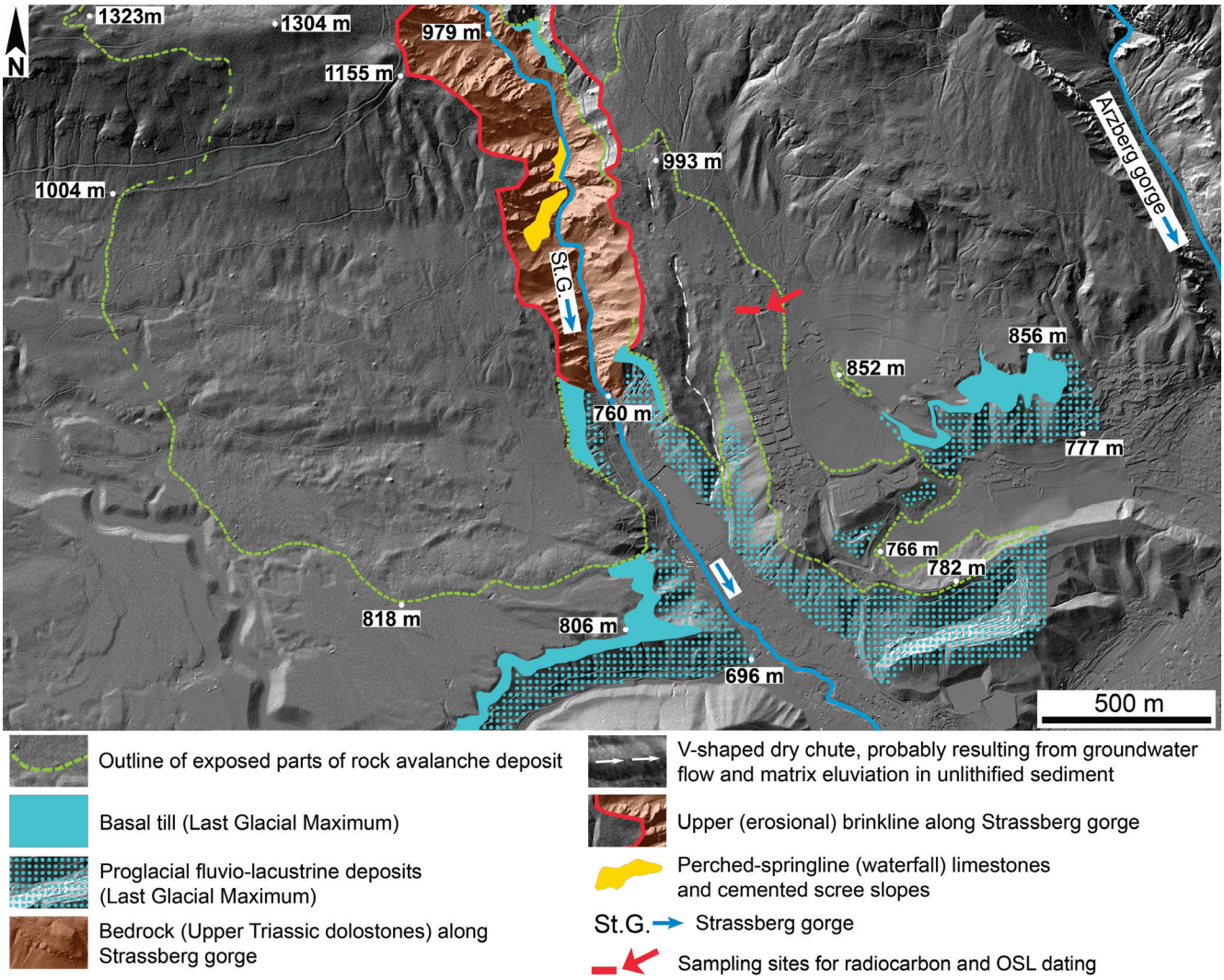

Figure 3: Geological map of the lower part of Strassberg valley. Note the thick proglacial–glacial succession of the LGM that buried the bedrock plateau with the present gorge exit. Along its distal right (point 818 m) and distal left part (near points 766 m and 852 m), the rock avalanche deposit is anthropogenically modified. Adjacent east of the gorge, linear chutes with a V-shaped cross-section are incised into the RAD and the underlying glacial–proglacial succession. The chutes are forested (pine, juniper) and do not show evidence for surface runoff. Short red bar indicates area of radiocarbon samples and of OSL sample (cf. Fig. 12D and E, Table 3).

Deposit type	Characteristics	Interpretation, references
Talus breccias	Stratified clast-supported breccias supplied from local cliffs Stratal dip 20-35°	Breccias accumulated from scree slopes supplied from local rock cliffs Sanders et al. (2009, 2010)
Proglacial fluvio-deltaic succession	(a) Foreset-stratified pebbly alluvium; foresets: 140/20-30° and 200/20-30° (b) Horizontally stratified pebbly alluvium; pebbles from NCA and from metamorphic rock terrains along Inn ice stream Successions overlain by LGM till	Succession (a): Fan delta debouching into proglacial lake; Succession (b) accumulated from proglacial outwash Ampferer (1904), Penck and Brückner (1909), Poscher (1993), Herbst et al. (2009)
LGM basal till	Matrix-supported diamicton with clasts from the NCA and from metamorphic terrains along the Inn ice stream; many clasts faceted, polished and striated.	Basal till of Inn ice stream of the LGM Ampferer (1904), Poscher (1993), Herbst et al. (2009)
Deglacial alluvial fan	Steep-dipping fan of pebbly alluvium of angular-subrounded clasts of WL; fan is 'detached' from its supply area of WL by the Arzberg gorge.	Alluvial fan supplied by runoff over downmelting ice from the southern cliffs of Mt. Hohe Munde (composed of WL)
Late-glacial moraines	Elongate high-standing sediment bodies parallel to valley thalweg; sediment is clast-supported, pebbly to bouldery with (scarce) matrix of carbonate-lithic sand to mud; clasts angular-subangular and derived from local rock substrate	Lateral moraines of late-glacial glaciers supplied from local cirques Well-developed in Alpl valley Senarclens-Grancy (1938)

Table 2: Quaternary deposits of study area. LGM=Last Glacial Maximum; NCA=Northern Calcareous Alps; NAR=Northern Alpine Raibl beds; WL=Wetterstein Limestone.

Deposit type	Characteristics	Interpretation, references
Rock avalanche deposit	Sheet a few dm to 65 m thick of extremely-poorly sorted pebbles to mesoliths of WL Lower part: fitted clast fabrics, in-situ fragmented clasts Upper part: disordered clast fabric with boulders, mesoliths on top	Rock avalanche detached from W cliff of Mt. Hohe Munde Ampferer and Ohnesorge (1912): "blocky till"; this paper: rock avalanche
Drape of loess	Regional sheet typically a few decimeters in thickness of polymictic siliciclastic silt. Found in study area from Mieming Plateau (800-850 m a.s.l.) up to LGM nunatak of Mt. Hohe Munde (2662 m a.s.l.)	Regional drape of loess accumulated during to shortly after ice decay (Gild et al., 2018)
Alluvial fans and scree slopes	(a) Large alluvial fans at exit of Strassberg and Arzberg valley (b) Higher-positioned systems: Upslope from (i) few degrees to ~15° dipping pebbly alluvium to (ii) steep-dipping (25-40°) scree slopes Small alluvial fans 'perched' high on scree slopes develop by trenching of talus apices	Alluvial fans and scree slopes supplied from local rock cliffs May contain rare clasts of metamorphic rocks derived from reworking of LGM glacial drift
Colluvium	Stratified intervals up to ~1 m thick of pebbly sand to sandy pebbles; NCA-derived clasts and metamorphic rock fragments Matrix: mixed siliciclastic/carbonate-lithic sand to silt Overlain by topsoil	Colluvial deposits accumulated from ephemeral runoff during late-glacial to historical times. Deposits probably formed at different times in limited areas (e.g., after forest fires or deforestation and/or during events of exceptional overland flow).
Spring limestones and cemented scree slopes	Perched springline along ~900 m a.s.l. along right flank of Strassberg gorge: waterfall tufas and cemented scree slopes along the base of the gorge	Spring limestones presently form at slow pace; U/Th age of cement in cemented scree slope: 9 ± 1 ka (Sanders et al., 2010)

Table 2: Continued.

valley, two stands of lateral moraines can be assigned to late-glacial valley glaciers, but their age is elusive (Fig. 3, Table 2). Surface exposure dating indicates that in particular in the NCA it is hardly possible to correlate specific stadials with altitudes of glacial moraines (cf. Moran et al., 2016). The central part of the study area is characterized by the RAD (Figs. 2, 4; Table 2). Because the RAD is of early late-glacial age (see below), it became partly downlapped by younger alluvial fans and scree slopes. In addition, in the distal part of the RAD east of Strassberg gorge, upon amelioration to gain acre, coarse blocks were blasted and removed over centuries. Together, these changes render the RAD less obvious than similar deposits in the environs (cf. Fig. 1).

4.2.3 Holocene

The present upper treeline in the study area is mainly controlled by distribution of rocky slopes and scree slope activity. Aside of bare rock cliffs, a few areas higher than ~1700-1800 m a.s.l. are covered by dwarf pines. Active scree slopes are largely confined to >1500 m a.s.l. along the proximal reach of Alpl valley; lower-positioned scree slopes are inactive and stabilized by vegetation. The present geomorphic activity in the study area is chiefly related to: (a) rockfall- and offwash-related sediment supply from cliffs onto scree slopes; (b) snow avalanches carrying clasts up to boulder size down to valley floors; (c) incision of Quaternary deposits by torrential runoff, and (d) headward erosion of the Strassberg gorge.

On the 22nd of March 2012, a 75.000 m^3 rockfall detached from Mount Hochwand (Fig. 2). The rockfall hit a scree slope covered with coarse-granular snow, and rapidly evolved into a 2.5 km-runout, 'two-layer' scree/snow avalanche (Figs. 2, 4) (cf. Sanders et al., 2014). The deposit and the kinematics of this rockfall have been analyzed previously and are not re-iterated in detail here (Preh and Sausgruber, 2014; Sanders et al., 2016). In the following, results with respect to selected Pleistocene deposits and to the bedrock gorges of the study area are presented.

5. Results

5.1 Deglacial scree accumulation and ravine incision

The SW-dipping slope of Schafkopf (1500 m a.s.l.) beyond the right brinkline of Arzberg gorge is veneered by a fan-shaped body of pebbly alluvium (Fig. 5). The fan overlies a truncated Upper Triassic succession and, locally, glacial till of the LGM. The fan consists of angular to subrounded clasts of Wetterstein Limestone (cf. Table 1) as it is present only a few hundreds of meters to the NE, along the left flank of Arzberg gorge (Figs. 2 and 5A). The fan sharply ends along the right brinkline of the gorge; the elongate depositional lobes on the fan surface converge towards a former point source to the north. This indicates that the Wetterstein-clastic material was derived from a gorge-like ravine within the southern cliff of Mount Hohe Munde (Figs. 5B and 6). In roadcuts and natural exposures, a thickness of the fan of at least a few meters is seen, but its base was not exposed. Aside of clasts of Wetterstein Limestone, in the distal part down from 900 m a.s.l., the fan is fringed by smaller depositional lobes that also contain a few clasts of metamorphic rocks.

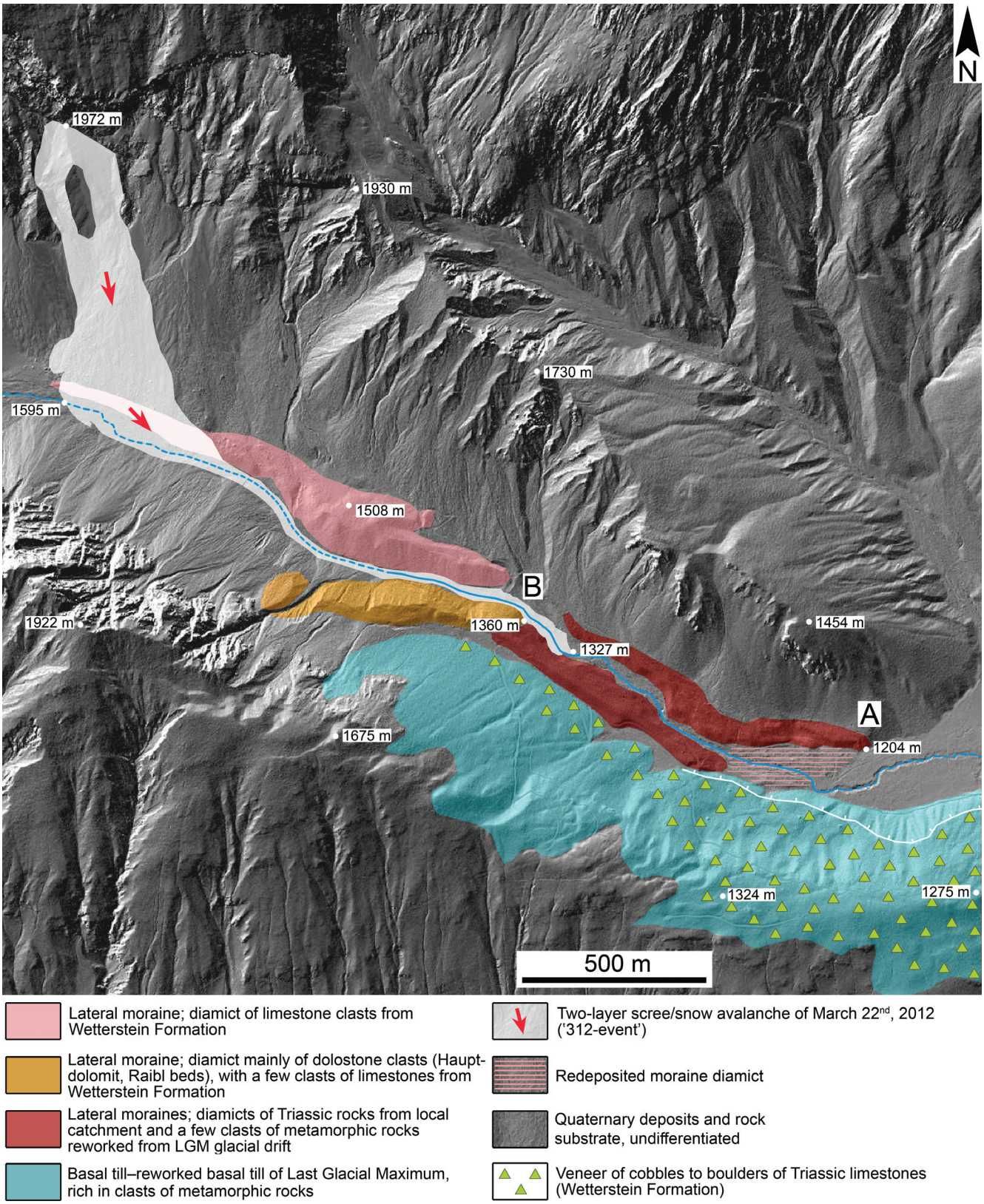

Figure 4: Geological map of the lower part of Alpl valley (cf. Fig. 2). The thalweg is flanked by lateral moraines stands (A, B) of late-glacial glaciers. The right valley flank consists of Hauptdolomit (cf. Table 1) covered by basal till/reworked basal till of the LGM, or by scree slopes. The valley flank is littered with cobbles–boulders of Wetterstein Limestone derived from a rock avalanche descended from Mt. Hohe Munde (cf. Fig. 2). The light grey area shows the runout of a 75.000 m^3 rock/snow avalanche on 22nd of March 2012.

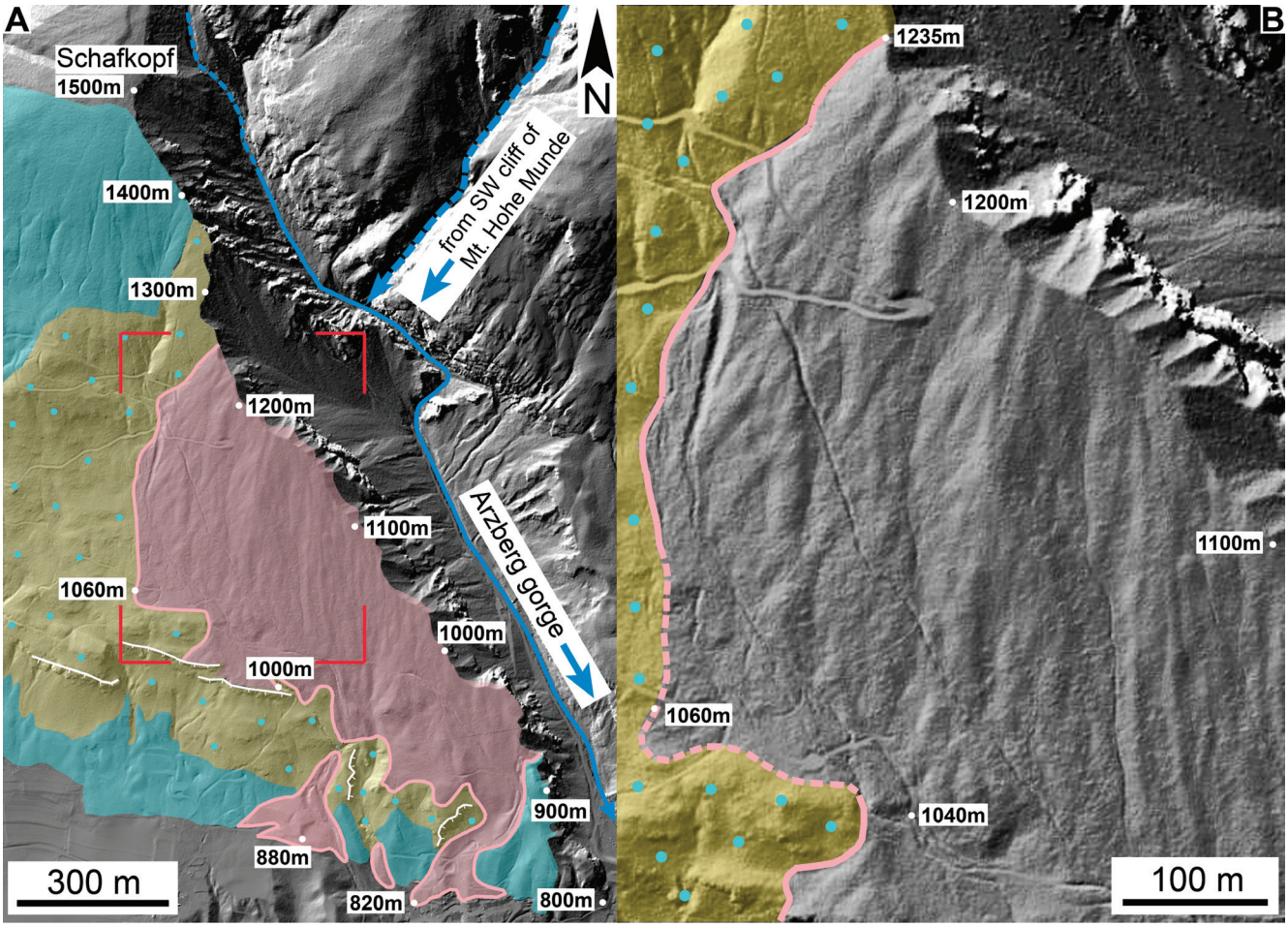

Figure 5: (A) S flank of Schafkopf (1500 m) beyond right brinkline of Arzberg gorge. The right-hand gorge flank consists of Hauptdolomit (Fig. 2, Table 1) veneered by LGM till, or that exhibits a mosaic of small rock outcrops, colluvium of Hauptdolomit debris, and LGM till. The S part of slope is veneered by an alluvial fan of clasts of Wetterstein Limestone building the left (opposite) gorge flank (cf. Figs. 2 and 6). Red rectangle: Outline of subfigure B. (B) Upslope, the depositional lobes of the alluvial fan (shown uncoloured to display surface) converge towards a former point source provided by a gorge-like ravine along the SW slope of Mt. Hohe Munde (cf. Figs. 2 and 6).

NW of the upper end of Arzberg gorge, the summit cliffs of Mount Hohe Munde are directly connected with a scree slope sculpted by incised ravines (Fig. 7). At several locations along the ravines, LGM basal till rich in clasts of metamorphic rocks is preserved. The till, in turn, is overlain by a package up to at least 50 m in vertical thickness of scree. In the stratigraphically deeper part of the succession, local intervals rich in clasts of metamorphic rocks with a matrix of mixed calcareous-micaceous siliciclastic sand to silt are present (e.g., near altitude point 1239 m in Fig. 7). Up-section, the scree succession becomes richer in clasts of Wetterstein Limestone, whereas clasts of metamorphic rocks become very rare. The stratigraphically upper part consists of moderately-sorted, stratified scree. The surface of the scree slope is sculpted by several 'generations' of mutually cross-cutting channels that became cut progressively deeper, down to the level of the presently active channels. The older channel reaches today are inactive and vegetated, and are perched in elevated positions relative to present thalwegs. Two of the ravines terminate into an alluvial fan shed over the RAD (Fig. 7). The deepest ravine, in turn, has near-permanent runoff in its lower part, and today is incised into the rock avalanche.

5.2 Rock avalanche

5.2.1 Overview and key parameters

The RAD comprises a veneer of extremely-poorly sorted, angular, pebble- to mesolith-size clasts of Wetterstein Limestone. Over its entire extent, the RAD overlies a rock substrate of Hauptdolomit (Fig. 2). Depending on location, the RAD is sandwiched between (i) bedrock or older Quaternary deposits (e.g., LGM basal till) below and (ii) younger sediments (e.g., alluvial fan deposits, loess,

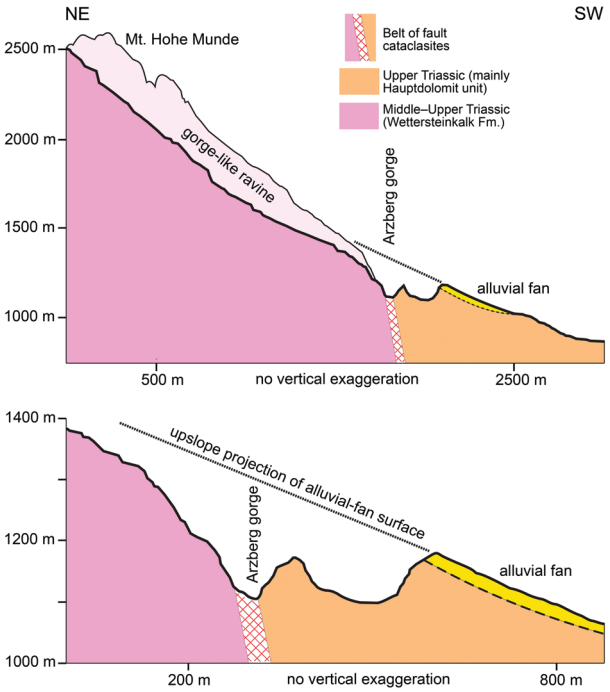

Figure 6: Section across Arzberg gorge (see dashed line 1-2 in Fig. 2 for trace), showing the rock substrate and the surface of the alluvial fan that consists exclusively of clasts of Wetterstein Limestone (cf. Fig. 5). Prolongation of the top of the alluvial fan indicates that the limestone debris was derived from the southern cliffs of Mt. Hohe Munde and shed across the Arzberg gorge. See text for discussion.

colluvial deposits) and/or topsoil above (Fig. 7). Many of the boulders to mesoliths projecting from the RAD had disintegrated by physical weathering into small, vegetated hillocks herein termed "tumuli" (from Latin: *tumulus* = gravehill).

The rock avalanche detached from the high western cliffs of Mount Hohe Munde (see Fig. 2). This is indicated by: (a) a distinct lunate scar in the western cliff (Fig. 8A), (b) composition of the RAD exclusively of clasts of Wetterstein Limestone, and (c) the runout path of the rock avalanche (Figs. 2, 9). A GIS-based estimate of the rock volume V detached from the scar amounts to ~11 Mm^3 (Fig. 8B). The fahrböschung angle α along a track corresponding to runout path E (Fig. 9) was determined at ~16° (inset in Fig. 2). The rock avalanche thus is within the range of typical V/α ratios of other catastrophic slope failures (cf. Collins and Melosh, 2003, their Figure 1). In descend, the rock avalanche was split into three 'branches': (a) a branch than ran up Alpl valley, corresponding to runout path A in Figure 9, (b) a branch that overran a mountain ridge right opposite of the detachment scar, corresponding to runout path B-C-D in Figure 9, and (c) a branch that ran out more-or-less unimpeded down slope, corresponding to runout path E in Figure 9. The following description of the RAD follows an outcrop-based subdivision into a proximal and distal part, respectively.

5.2.2 Proximal part

The most proximal exposed part of the RAD is (i) partly buried under younger deposits of the Strassberg intramontane basin, and is (ii) downlapped by alluvial fans and scree slopes shed from the W flank of Mount Hohe Munde (Figs. 2, 7). On the mountain ridge of Hauptdolomit SW of the Strassberg basin, roadcuts and natural exposures allowed to track the RAD. In this area, mesolith- to boulder-sized clasts of Wetterstein Limestone project from a basal veener of smaller-grained Wetterstein-clastic material. Nowhere in this area evidence was found that the RAD would comprise a cover more than, at most, a few meters in thickness.

The best section through the RAD is exposed along a left-hand tributary to Strassberg gorge, up from 970 m a.s.l. (Figs. 7, 10). Here, a truncation surface cut into Hauptdolomit is overlain by strongly compacted till. The till is rich in faceted, polished and striated lithoclasts; the clasts are derived from the NCA and from terrains of metamorphic rocks in the upstream catchment of the Inn river (e.g., garnet amphibolites, retrograde eclogites, orthogneiss with greenish feldspars) (Fig. 11A). This till is overlain by the purely Wetterstein-clastic deposit of the RAD (Fig. 11B). In its basal and lower part, the RAD is a densely-packed, extremely-poorly sorted, clast-supported deposit. Clasts are up to boulder size, and many of them show a tightly interlocked clast fabric fitted along fracture surfaces, also across clasts of boulder size (Fig. 11C). The scarce matrix is white cataclastic gouge rich in angular fragments of Wetterstein Limestone (Figs. 11D and 12E). Up-section, towards the topmost levels of the RAD, clast fitting disappears into a disordered clast fabric, and the deposit contains mesoliths of Wetterstein Limestone floating atop (Figs. 11F and 12A). Along the lower side of exposed mesoliths, 'underboulder breccias' of lithified rock-avalanche material locally are present (Figs. 12A, 13B and C). The total thickness of the RAD in this section is at least 70 m. Downstream of the described section, the RAD gradually thins due to relative rise of the top of bedrock to a veneer a few meters to 10 m in thickness along both flanks of the gorge (Fig. 3). Along most of the orographic right flank of Strassberg gorge, due to dense forestation and downslope redeposition of both RAD and underlying till, the boundary between till and RAD can hardly be placed with certainty.

5.2.3 Distal part

The distal part of the RAD is well-identifiable by projecting boulders to mesoliths of Wetterstein Limestone. On the plateau right of Strassberg gorge, the RAD comprises a laterally discontinuous veneer — interspersed with boulders to mesoliths partly degraded to tumuli — typically a few decimeters to a few meters in thickness that overlies till/reworked till. This area is characterized by a complex surface morphology (Figs. 3 and 12). Near its westernmost tip, the RAD plus underlying till are involved in slumping (Fig. 13A). In the central part of the area, elongate morphological depressions (probable slump scars) are floored by stratified colluvium. Furthermore, the central part of the area displays an irregularly hummocky morphology. In the lower part, the RAD is locally

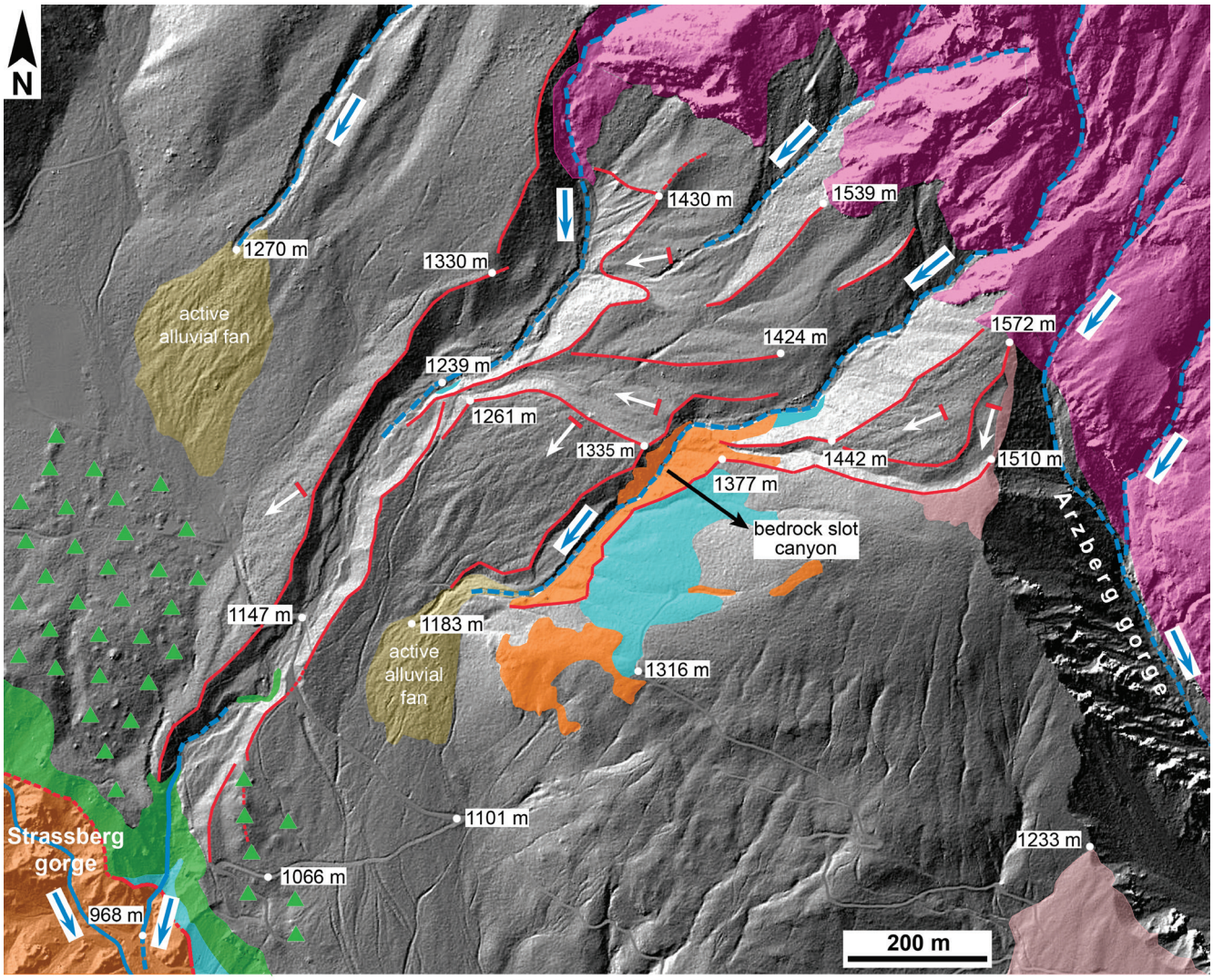

Figure 7: Geological map of the lower SW slope of Mt. Hohe Munde (cf. Fig. 2). A thick scree-slope succession is sculpted by successive 'generations' of incised channels (white arrows) today perched in elevated positions relative to the presently-active ravines. Erosion supplies alluvial fans that prograde over the rock-avalanche deposit. Despite only ephemeral runoff, along the southern ravine, a small bedrock slot canyon became incised into dolostones.

veneered by stratified colluvium (Fig. 13A). The colluvium is rich in micaceous sand of mixed siliciclastic/carbonate-lithic composition; the lithoclast fraction includes pebbles of metamorphic rocks and of rocks derived from the NCA. The slope directly upward of this 'colluvial plain' is littered with cobbles to boulders of Wetterstein Limestone (rock-avalanche material), but clasts of metamorphic rocks also are found (Fig. 13A); still higher up, slope facets excavated from and incised into both the till and the overlying RAD are present (Fig. 3). Near the distal end of the RAD, raised elongate features of a relief amplitude of 5-7 m are present; these features are oriented oblique to transversal to rock-avalanche flow ('esker-like features' in Fig. 13A). Near the distal end, the surface of the RAD is sculpted into faint arrays of strongly elongate ('linear') furrows and ridges parallel to the propagation direction of the rock avalanche; high-resolution sections show that the ridges typically show an elevation of 1-2 m relative to the intercalated furrows (Figs. 13B and C).

Beyond the left brink of Strassberg gorge, construction pits excavated between 850–880 m a.s.l. provided outcrops of the RAD and overlying deposits. Here, the RAD is a clast-supported Wetterstein-clastic deposit with a scarce matrix of cataclastic gouge. Fitted clast fabrics are absent, and clasts are angular and show numerous impact marks on their surface. In these outcrops,

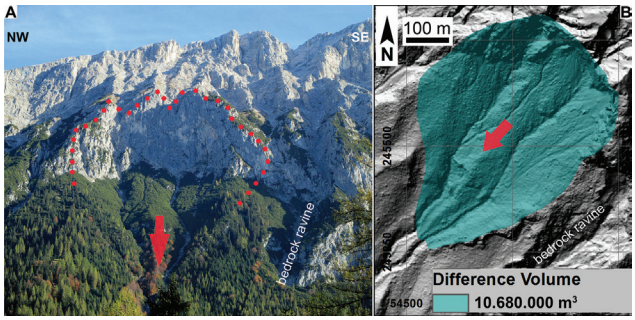

Figure 8: (A) View into detachment scar of rock avalanche. Because of a high post-glacial age (see text) of the rock-avalanche event, the scar became lichenized and overprinted by later erosion. Therefore, the outline of the scar as shown by the red stipples is a proxy only. (B) LIDAR topography showing detachment scar used for GIS-based volume estimate of 11 Mm^3 of the rock avalanche.

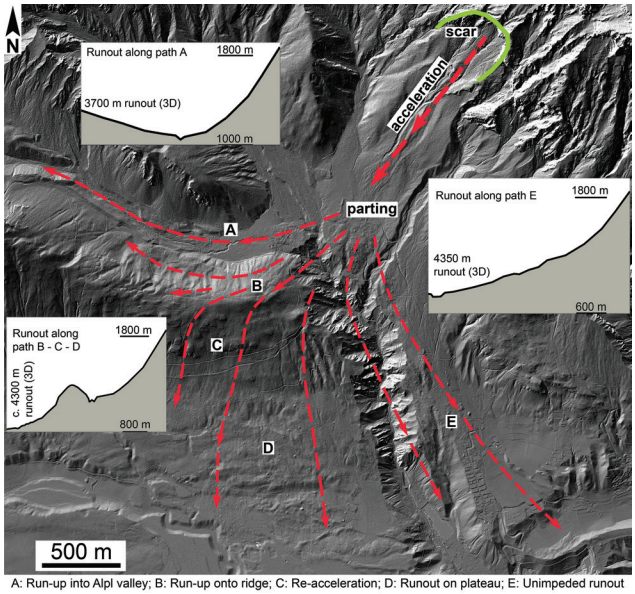

A: Run-up into Alpl valley; B: Run-up onto ridge; C: Re-acceleration; D: Runout on plateau; E: Unimpeded runout

Figure 9: Approximate trajectories of rock avalanche runout (Lidar data). After detachment and acceleration, the rock avalanche was parted into three branches by an opposite mountain ridge.

the RAD is up to ~6 m in thickness at least (base not exposed, Fig. 12D); it is overlain by colluvial deposits and intercalated soils that provided an opportunity to *ante-quam* radiocarbon date the mass-wasting event. The highest age of 11.18-11.17 ka cal BP was determined for a soil sandwiched between two colluvial intervals (Fig. 12E, Table 3). A layer of loess directly above the RAD (Fig. 12E inset) was sampled for OSL dating; the layer yielded a quartz OSL age of 18.77 ± 1.55 ka (Table 3) (Gild et al., 2018).

6. Bedrock gorges

6.1 Strassberg gorge

Along the downslope end of the Strassberg intramontane basin, the valley floor is a few hundreds of meters in width, yet the present drainage runs in a gorge (Fig. 2). The stream that drains the gorge is sourced from several tributaries that are incised into and emerge from

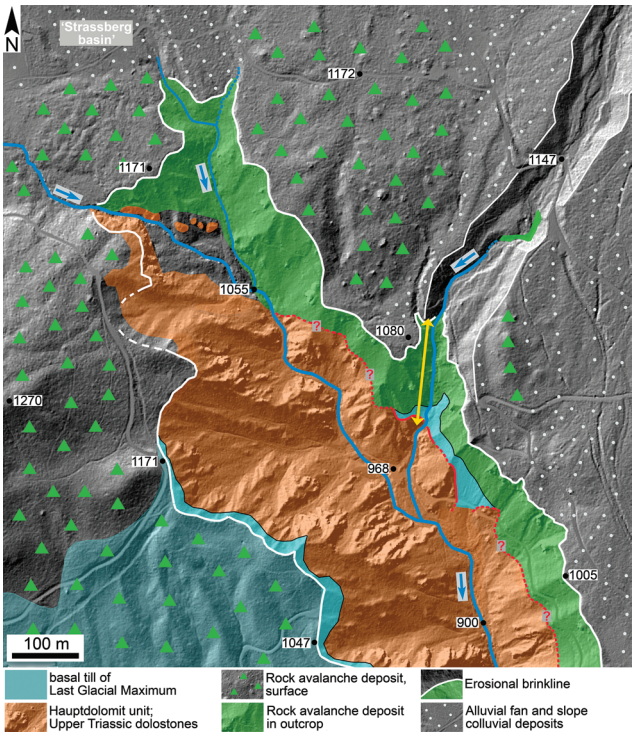

Figure 10: Upper part of Strassberg gorge (Lidar data). The stream is incised into Hauptdolomit (cf. Table 1) and, in its headward ephemeral reach, into the rock avalanche deposit. On the orographic left bank, the rock avalanche is downlapped and partly buried by alluvial fans (cf. Fig. 6). Yellow line marks the succession illustrated in Figure 11A-F and Figure 12A-C.

the intramontane basin filling (Fig. 10). Each tributary shows a bouldery cascade channel to step-pool channel. Downstream, both flanks of the gorge are progressively deeper incised into bedrock (Fig. 10). In the upstream part of Strassberg gorge, the top of bedrock along the right flank is distinctly higher than along the left flank (Fig. 14A and B). This asymmetry of left/right bedrock brinklines tapers out from ~900 m a.s.l. and downstream thereof, where the gorge is incised into the rock-cored Mieming Plateau (cf. Figs. 2, 3, 14C and D). In the area of cross-sections C and D, the stream incision into Hauptdolomit rock is down to ~90–120 m.

Along the right gorge flank, a perched springline at 890-905 m a.s.l. supplies an array of waterfall tufas (Fig. 3). Upvalley, the springline terminates where it merges the intersection with the gorge thalweg; downstream, springs taper out near the intersection with the till/RAD-covered Mieming Plateau (Fig. 3). *In-situ* experiments (1.4.2005–24.9.2005) and checks of precipitation substrates (August 2000–July 2006) indicate that limestone deposition presently proceeds at a very low rate. The former limestone-depositing springs had cemented small talus cones up to 6 m in preserved vertical thickness (Fig. 12F). Today, all of the cemented scree slopes are erosional relicts that were graded to base-levels a few meters above the present stream. In an outcrop 3.6 m above the present stream level, an erosional remnant of cemented pebbly alluvium is downlapped by talus breccias. A sample of cement from lithified talus ~6 m above the present stream level yielded

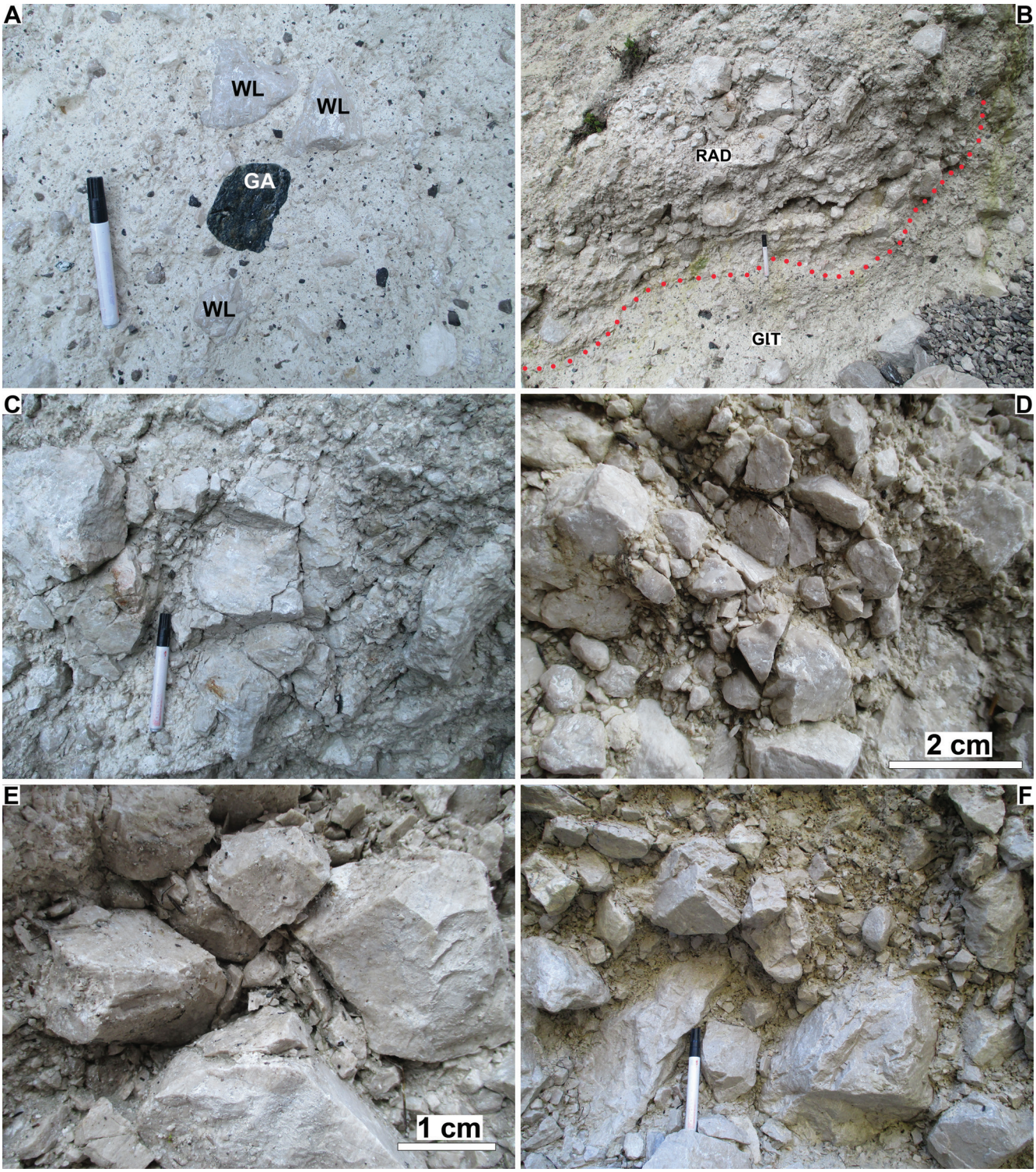

Figure 11: Outcrop photographs. (A) Strongly compacted, matrix-supported till with clast of garnet amphibolite (GA), and rich in clasts of carbonate rocks from the Northern Calcareous Alps (WL=Wetterstein Limestone; cf. Table 1). Pen: 14 cm. (B) Boundary (stippled) between glacial till (GlT) below and rock avalanche deposit (RAD) above. Pen: 14 cm. (C) Basal part of rock avalanche deposit of clasts of Wetterstein Limestone. Note: (a) extremely poor sorting, (b) whitish cataclastic matrix, and (c) *in-situ* fractured lithoclasts. Pen: 14 cm. (D) Basal part of rock avalanche deposit. Note: (a) scarcity of cataclastic matrix, and (b) fitted clast boundaries. (E) Interstitial clast space of basal part of rock avalanche. Note matrix of angular rock chips. (F) Rock avalanche deposit ~30 m above its base. Note disordered fabric and absence of clasts fractured *in situ*. Pen: 14 cm.

a mean $^{234}U/^{230}Th$ disequilibrium precipitation age of 9 ± 1 ka (Sanders et al., 2010). Along its entire length, Strassberg gorge is floored with an alluvial channel. Pool-riffle and step-pool channels prevail in the distal sector of the gorge, but short reaches with cascade channels are intercalated, depending on local presence of boulders derived mainly from rockfalls and topplings from the gorge flanks. At its downstream end, the bedrock gorge sharply terminates at a subvertical rock cliff that became buried under proglacial and glacial deposits (Fig. 3).

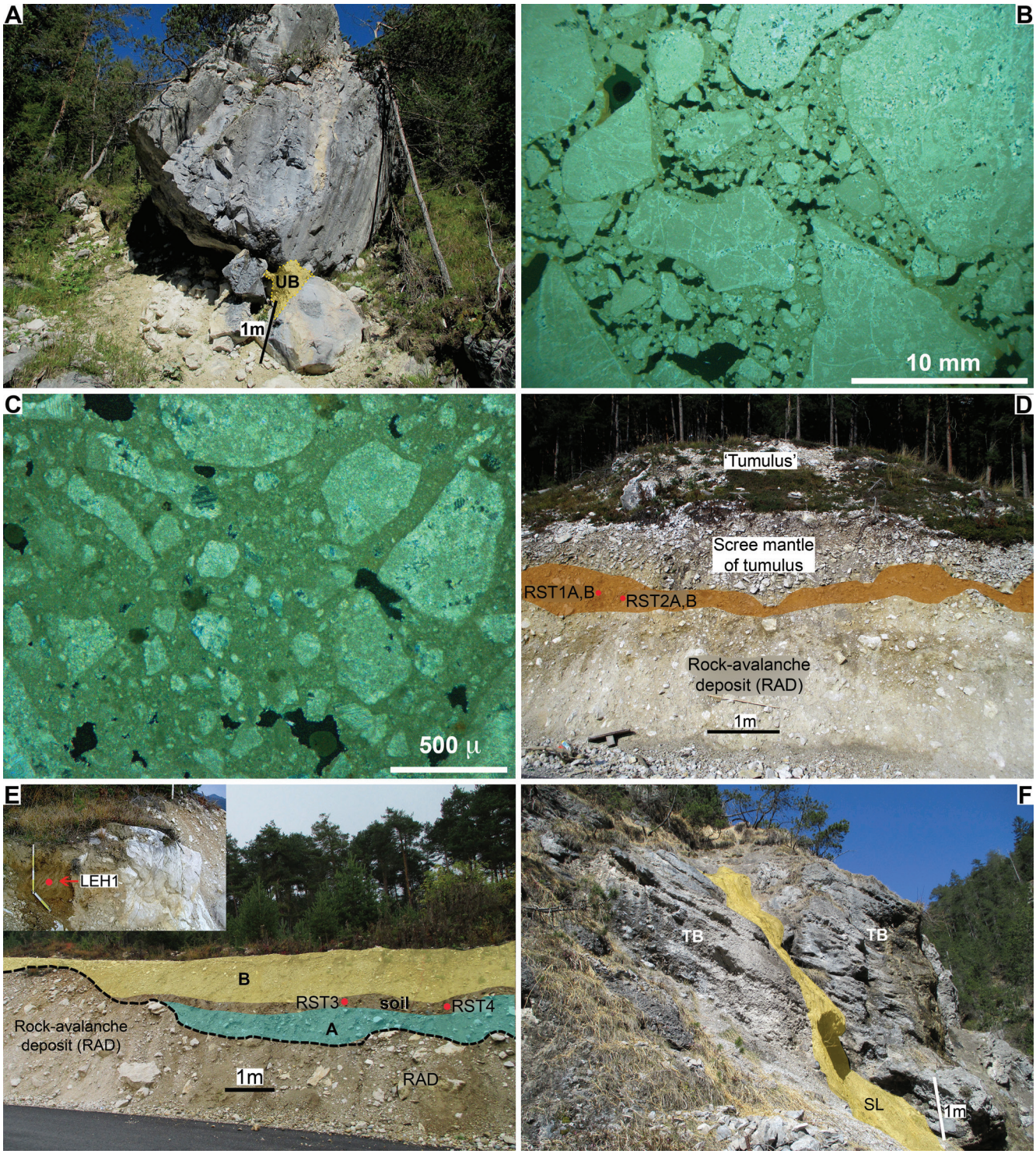

Figure 12: Outcrop and thin section photographs. (A) Mesolith on top of rock avalanche deposit. Underboulder breccia (UB) highlighted yellow. (B, C) Thin section images of underboulder breccia of subfigure A. Note: (a) extremely poor sorting, (b) matrix of ultracataclasite (grey), and (c) open pores (black). Crossed nicols. Widths of view: 29 mm (B); 2.2 mm (C). Note 'self-similar' clast-size distribution in both images. (D) Anthropogenic pit into RAD, 880 m a.s.l. (cf. Fig. 3 for location). An interval of silty organic-rich loam (highlighted brown) above the RAD was sampled for radiocarbon dating (red dots). The organic-rich loam is buried beneath a scree apron formed by physical weathering of a mesolith of Wetterstein Limestone to a tumulus. (E) Anthropogenic pit into RAD and overlying colluvial intervals (A, B), 880 m a.s.l. (cf. Fig. 3 for location). A soil intercalated between the colluvial intervals was sampled for radiocarbon dating (red dots). Inset: Sampling location of OSL sample LEH1 from a drape of loess directly above the RAD. (F) Relict of talus breccia (TB) and active spring limestone (SL, highlighted yellow) on right flank of Strassberg gorge.

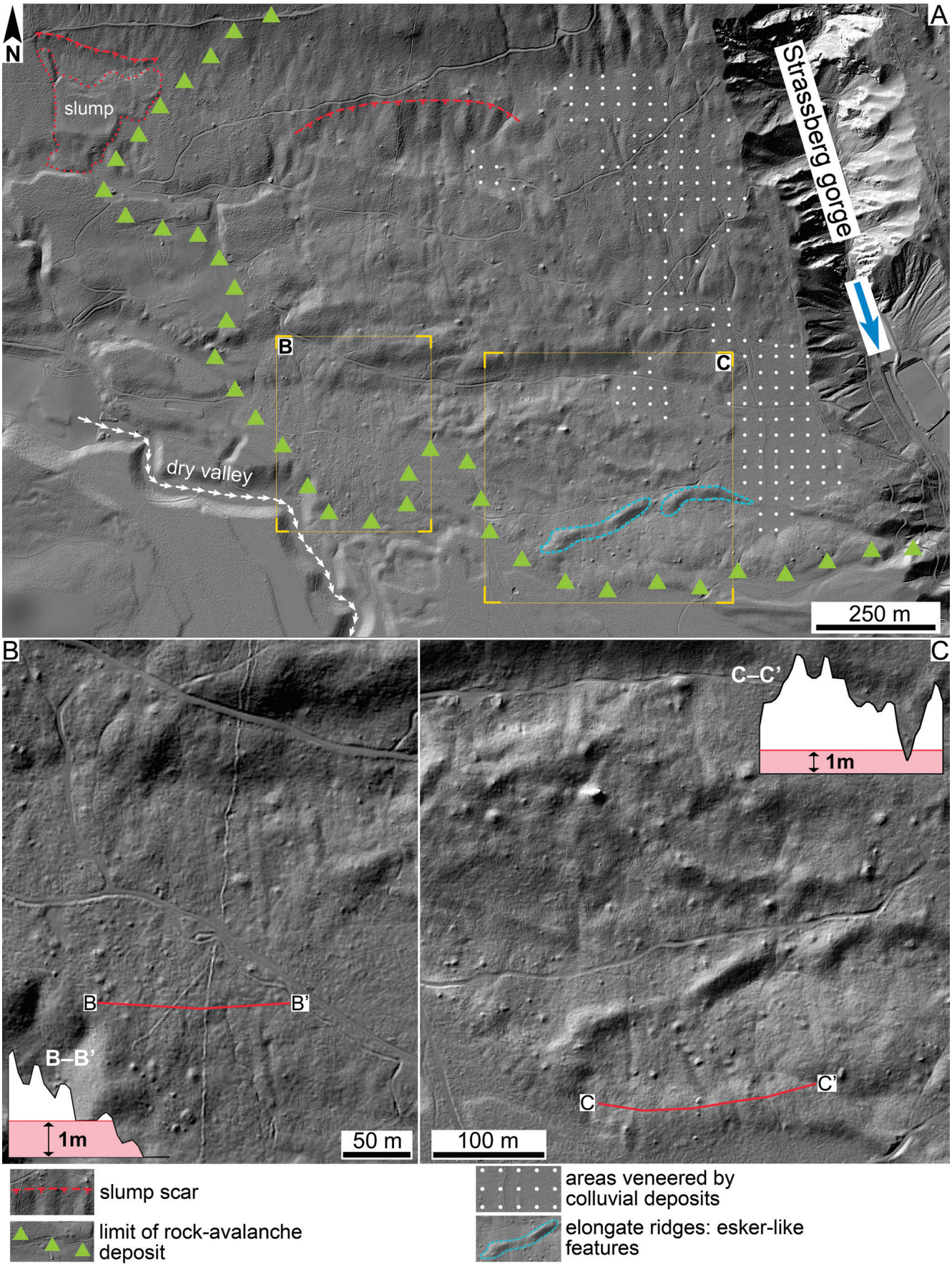

Figure 13: Lidar data. (A) Surface morphology and extent of RAD west of Strassberg gorge. (B, C) Details showing arrays of elongate ridges and furrows parallel to the local propagation direction of the rock avalanche. Insets show high-resolution topographic sections (vertically exaggerated, horizontal scaling same as plan-view bars) along the red traces B-B' and C-C'.

Sample code, lab ID, location	Field presence	Age, 2σ calibrated BP1950, Figure reference
RADIOCARBON AGES		
RST 1(A), BETA 401694, N47°19′27.37″/E11°03′19.42″	Soil below scree mantle of rock-avalanche tumulus(1)	**(a) cal 1180-1050 BP; (b) cal 1025-1005 BP** Fig. 12D
RST 1(B), BETA 401695, N47°19′27.37″/E11°03′19.42″	Soil below scree mantle of rock-avalanche tumulus	**cal 1885-1730 BP** Fig. 12D
RST 2(A), BETA 401696, N47°19′27.37″/E11°03′19.42″	Soil below scree mantle of rock-avalanche tumulus	**cal 2310-2120 BP** Fig. 12D
RST 2(B), BETA 401697, N47°19′27.37″/E11°03′19.42″	Soil below scree mantle of rock-avalanche tumulus	**(a) cal 1300-1260 BP; (b) cal 1200-1190 BP** Fig. 12D
RST 3, BETA 401698, N47°19′27.50″/E11°03′24.08″	Soil sandwiched between reworked glacial till and NCA-derived colluvial pebbly deposit	**cal 8035-7960 BP** Fig. 12E
RST 4, BETA 401699, N47°19′27.50″/E11°03′24.08″	Soil sandwiched between colluvium of reworked LGM till and overlying NCA-sourced colluvium	**(a) cal 11180-11170 BP; (b) cal 10950-10807 BP** Fig. 12E
Quartz OSL AGE		
LEH1_OSL1 Lab ID number: L012/2, N47°19′27.64″/E11°03′17.31″	Well-sorted siliciclastic silt directly on rock-avalanche deposit, sample taken 40 cm below top	**18.77 ± 1.55 ka** Inset in Fig. 12E

(1) tumulus: boulder more-or-less disintegrated into scree by physical weathering while resting in place.

Table 3: Numerical ages (radiocarbon, OSL) used to constrain the age of the rock-avalanche event. Radiocarbon ages are from acid-washed fraction of soil levels above the rock avalanche deposit, location Sonnensiedlung (840 m asl) near Telfs.

6.2 Arzberg gorge

The incision of Arzberg gorge follows two fault sets (Fig. 2). Near their intersection, the faults are associated with sub-vertical damage zones up to more than 15 m in thickness of layered and stylolitized cataclasites to ultracataclasites. At its debouch onto an alluvial fan, the gorge is incised into low cliffs of Hauptdolomit; upstream, the incision increases to maximum depths of 150–170 m. Most of the lower sector of the stream is captured in a concrete channel with run-of-river dams. Upstream of 950 m a.s.l., however, a bedrock channel incised into cataclasites is present.

As described, the mountain flank beyond the western brink of the gorge is veneered by an alluvial fan composed exclusively of clasts of Wetterstein Limestone (Figs. 5 and 6). On the slope beyond the eastern gorge brink, in contrast, a hummocky morphology that comprises a highly variable mixture of clasts of Wetterstein Limestone and LGM-glacial drift is present. Aside of bedrock flanks, the slopes that face into the accessible lower sector of Arzberg gorge consist of talus sourced from the underlying rock. Despite field mapping along the lower gorge sector, no geomorphological indication or sedimentary record could be found that in itself would provide a strong argument for a pre- or post-LGM origin of Arzberg gorge.

7. Interpretation and discussion

7.1 Late-glacial scree shedding and ravine incision

A graphic summary of the pre-last glacial to present development of the study area is given in Figure 15. The described remnant of a Wetterstein-clastic alluvial fan that was shed across Arzberg gorge, and perched along the left flank of Strassberg valley, indicates that during deposition, the fan must have been somehow connected to the SW cliffs of Mt. Hohe Munde (cf. Figs. 2, 5, 6 and 15C). To derive the clast composition of the fan, two hypotheses may be proposed: (1) the fan formed before the incision of Arzberg gorge (or a proximal reach thereof) that now separates the sediment provenance area from Mt. Hohe Munde from the accumulation area, or (2) the fan accumulated while a pre-existing Arzberg gorge was bridged by dead ice during deglacial ice collapse. Because of the position of the Wetterstein-clastic fan along the lower reach of Arzberg gorge, the first hypothesis would imply that the gorge as well as the bedrock canyon in the SW cliff of Mt. Hohe Munde formed nearly entirely after the LGM. It is considered improbable that Arzberg gorge formed entirely during the post-LGM interval; rather, a precursor gorge probably existed, albeit of shorter upstream extent. This precursor gorge was clogged with dead ice while copious sediment (scree, LGM glacial drift, clasts of talus breccias) was shed from the SW slopes of Mt. Hohe Munde, focused into the canyon, and transported over dead ice onto the left flank of Strassberg valley. The good preservation of the surface of the deglacial alluvial fan (Figs. 5A and 6B) indicates that, except for soil development and forestation, this slope remained nearly unmodified since deglacial ice collapse, i.e., it represents an element of the land surface roughly some 20–18 ka in age.

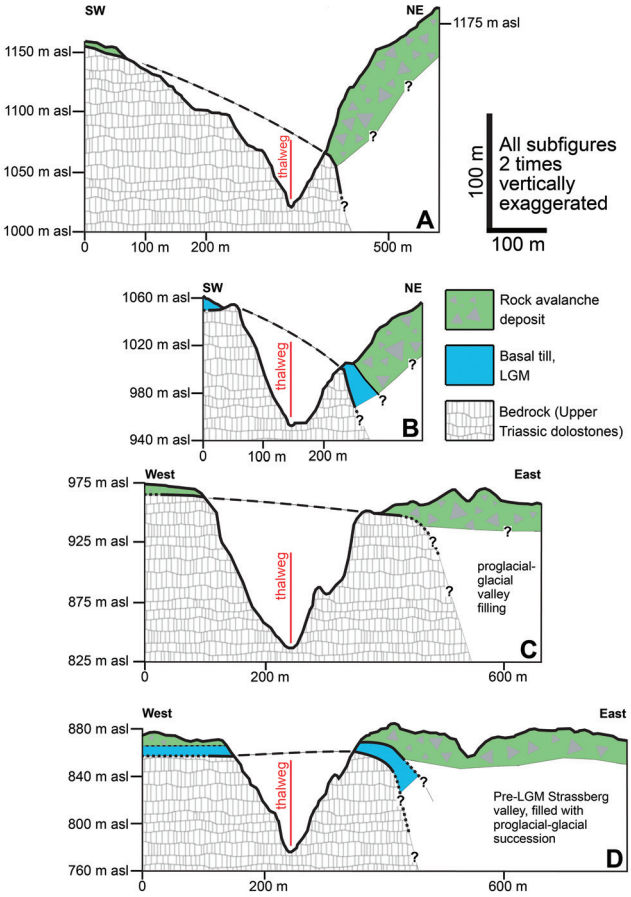

Figure 14: Sections across Strassberg gorge from upstream (section A) to downstream (section D) (see Fig. 2 for traces). In the upper gorge reach (sections A and B), the top of bedrock is located at distinctly different altitudes on each gorge flank. Downstream, towards the Miemingplateau (cf. Fig. 2), the bedrock tops are located on similar altitudes (sections C and D).

The observation that the thick alluvial fan and scree slope succession along the W slope of Mt. Hohe Munde downlaps and oversteps the RAD underscores that mass-wasting happened early after deglaciation (Figs. 7 and 15C). The described slope succession W of Hohe Munde records: (a) redeposition of glacial till and, perhaps, of ice-marginal meltout sediment rich in siliciclastic sand, succeeded by (b) progressive and effective shedding of Wetterstein-clastic material from the re-exposed rock cliffs, until purely carbonate-lithic scree slopes had formed, followed by a switchover to (c) progressive incision of erosional ravines into slopes stabilized by vegetation. This cycle from rapid deglacial-paraglacial slope aggradation to prolonged incision of ephemerally-active chutes is highly characteristic of the NCA (e.g., Sanders and Ostermann, 2011; Sanders, 2012). Further notable is the incision of a short bedrock slot canyon by ephemeral runoff along one of the ravines (see Fig. 7), favoured by the high erodability of the dolostones of the Hauptdolomit unit.

7.2 Rock avalanche deposit

The RAD was mapped last time by Ampferer and Ohnesorge (1912), who designated it as "blocky till" (German: *Blockmoräne*), i.e., as a glacial deposit formed during stadial ice retreat (German: *Ablagerung der Rückzugsstadien*). Veneers of boulders to mesoliths are common in the NCA, and were subsumed as *Bergsturzmoräne* ("rock avalanche till") or simply as *Blockstreu* ("littered blocks"). Except for the latter descriptive term, these designations reflect a conjectural association of mass-wasting with deglacial to late-glacial ice. This calls to argue why the deposit of the present study represents a rock avalanche rather than a till (Table 4).

A notable part of the RAD is the area west of Strassberg gorge (cf. Figs. 2, 3, 13). The irregular topography in this area may represent a hummocky moraine formed during deglacial ice decay. In addition, slumping of till and overlying RAD enhanced surface topography, and led to local thinning and even interruption of lateral continuity of the RAD. The colluvial veneers along the toe of slump scars and over gentle depressions accumulated from overland flow (Fig. 13); sizeable erosion after rock avalanching is also recorded by the slope facets excavated from, both, till and RAD (Figs. 3 and 13). The linear furrows and ridges (Figs. 13B and 13C) are reminiscent of flowbands. These features are typical of rock avalanches that spread and run out more-or-less freely, in many cases over snow or ice; in well-preserved RADs, flowbands extend over most of the deposit (see Hungr and Evans, 2004; Dufresne and Davies, 2009; Shugar and Clague, 2011). For the RAD described herein, however, the hummocky substrate and the overprint by post-depositional processes have led to poor development and/or poor preservation of potential flowbands. In addition, the kinematic history of the rock avalanche, involving a splitting of the mass and run-up onto a mountain ridge, impeded pervasive flowband development.

Notwithstanding local thinning of the RAD by slumping and creep, in the area W of Strassberg gorge, the good visibility of landforms of the overridden substrate (Fig. 13) suggests that at least in this part, the RAD is a few meters in thickness at most. This is confirmed by comparison to much thicker RAD in the environs of the study area (e.g., Tschirgant, Haiming, cf. Prager et al., 2008; Dufresne et al., 2015). In such a thin veneer, effective mechanical coupling from pebbles to mesoliths seems hardly possible even if the mass moved only by plug flow (compare Davies et al., 1999; Erismann and Abele, 2001; Davies and McSaveney, 2002, 2009; McSaveney and Davies, 2002; 2009; Locat et al., 2006; De Blasio and Crosta, 2014; Perinotto et al., 2015). Such a transport mode was possible, however, if the rock avalanche propagated on a layer of basally entrained snow. In case of unconfined movement, this enables long runout and/or lateral spread of thin sheets of mesolithic to bouldery debris. Only during the past few years, the common incidence of rock avalanches and large rockfalls propagating on layers of snow or ice became appreciated (e.g., Hungr and Evans, 2004; Pirulli, 2009; Jiskoot, 2011; Shugar and Clague, 2011; Hungr et al., 2012; Sanders et al., 2014, 2016; Preh and Sausgruber, 2015). After snowmelt, a deposit is left that

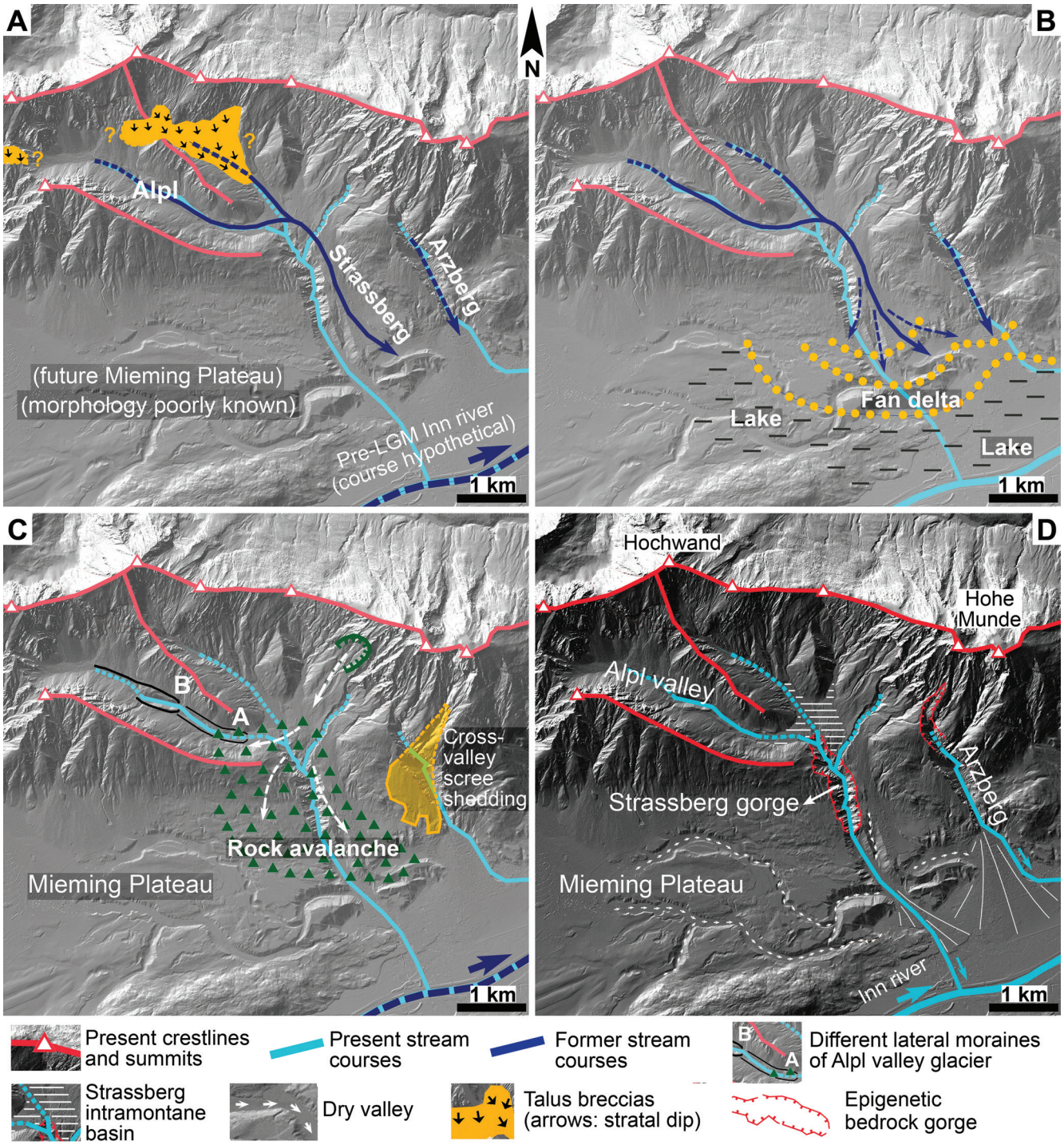

Figure 15: Landscape development. (A) Pre-LGM phase, including relicts of talus breccias of unknown age. The pre-LGM Strassberg valley followed a more eastern course. (B) Beginning of LGM. The Inn valley was occupied by a lake of unknown extent. A fan delta supplied from Strassberg and Arzberg valley prograded into the lake. (C) Deglacial to late-glacial. During ice collapse, an alluvial fan supplied from Mt. Hohe Munde prograded across Arzberg gorge (filled with dead ice) over the left flank of Strassberg valley. When Strassberg valley was still largely filled with sediment, an ~11 Mm^3 rock avalanche detached and set the base-level for an intramontane basin. In Alpl valley, late-glacial glaciers left two sets of lateral moraines. (D) The post-LGM drainage of Strassberg valley follows an epigenetic bedrock gorge. On the Mieming Plateau, proglacial to deglacial deposits became incised by valleys (now dry) that probably guided runoff during ice collapse.

may appear enigmatic with respect to its long runout and low thickness because a decisive mechanical component – the snow – has vanished. In the Eastern Alps, the number of identified deposits of highly mobile, former rock/snow avalanches steadily increases because the criteria how to identify them become increasingly clear (Sanders et al., 2016).

The quartz OSL age of 18.77 ± 1.55 ka of the loess layer directly above the RAD fits with geomorphological and sedimentological indicators that suggest a high late-glacial age of mass-wasting: (a) the RAD directly overlies LGM till; (b) the pre-LGM Strassberg valley was not or only partly cleared of its LGM-related sediment filling when mass-wasting took place; (c) the proximal part of

Deposit feature	Interpretation, references, figure reference	Remarks
Feature 1: Composition exclusively of clasts of WL	Derivation from crescentic scar in cliff of WL along SW face of Mount Hohe Munde Figs. 2 and 8	Basal till of late-glacial debris-rich glacier should contain all lithologies of catchment plus reworked clasts of metamorphites of LGM till
Feature 2: Lower part of deposit: clasts show fitted fabric; scarce matrix of cataclastic gouge	Fitted clast fabrics typical of rapid mass transport involving dynamic disintegration (e.g., Davies et al., 1999; De Blasio and Crosta, 2014; Perinotto et al., 2015) Fig. 11B and E	Basal till of late-glacial glacier should be diamicton with polished/striated/pressure-marked clasts, and should comprise all lithologies of catchment plus metamorphites of LGM till
Feature 3: Vertical transition from (a) fitted clast fabric via (b) disordered clast fabric with scarce matrix of cataclastic gouge into (c) top layer with mesoliths	Typical vertical transition of fabrics within rockslides and rock avalanches (e.g., Cruden and Hungr, 1986; Pollet & Schneider, 2004) Figs. 11B-F and 12A-C	Unknown from tills and moraines
Feature 4: Veneer of WL-clastic, extremely-poorly sorted, blocky deposit draping the Hauptdolomit-cored mountain ridge on the right flank of Alpl valley.	Run-up of rock avalanche detached from W face of Mount Hohe Munde onto opposite slope Figs. 2, 4 and 9	No such dynamic behaviour is known from glaciers; glacier should leave moraines

Table 4: Features indicative of rock-avalanche origin of described boulder- to mesolith-bearing deposit. WL=Wetterstein Limestone.

the RAD is overstepped by alluvial fans; (d) the RAD propagated while the Strassberg gorge still was not existent (Fig. 15C). The rock avalanche must post-date ~21 ka, when deglacial ice collapse started, and pre-date the quartz OSL age as given above; overall, the event may be bracketed to a maximum age range of ≤ 21 ka to ≥ 17.5 ka BP. As seen in Figure 2, the detachment scar is located near faults of large displacement. The rock avalanche thus may have detached in reaction to an earthquake, either along the Telfs fault system or elsewhere (cf., e.g., Jibson, 2013; Keefer, 2013), and/or due to other triggers such as prolonged intense rain or simply gravitational collapse resulting from glacial steepening of the cliff surface right along the fault. In any case, fault zones provide a combination of seismic shaking, deformation and rock disintegration along structural weaknesses, a combination that – in the long term – will lead to increased incidence of mass wasting. On the Mieming Plateau a few kilometers west of the study area, another bouldery veneer with flow-bands and a sharp snout is present (Number 2 in Fig. 1C); this veneer, previously viewed as a terminal moraine, was re-interpreted as a rock avalanche that probably rode on a substrate of snow or ice (Westreicher, 2014). The RAD described herein so far is the oldest age-dated post-LGM catastrophic mass-wasting of the Eastern Alps (see the age compilation in Prager et al., 2008).

7.3 Bedrock gorges

As described, the head of the Strassberg gorge is incised into bedrock and into the RAD (Fig. 10) which, in turn, provides the base-level to an intramontane basin. For the upper part of Strassberg gorge, the asymmetric heights of bedrock brinklines along the left and right flanks, and the basal till along the left flank suggest that the upper reach of the gorge is incised into a former bedrock valley flank (Figs. 10, 14A, 15B). At the exit of the gorge, the bedrock surface along the left flank dips steeply towards the East (Figs. 3, 14D). The V-shaped, dry chute incised into the RAD and, farther downslope, into the underlying LGM succession (Fig. 3) probably originated from eluviation by subsurface runoff within loose sediment (cf. Kampf and Mirus, 2013). The integrated evidence thus indicates that the present Strassberg gorge originated after the LGM, and that the former (pre-LGM) valley followed a thalweg farther towards the East (Fig. 15A and D).

The outcrops along the upper gorge reach (Figs. 10, 14B) and at the exit of the pre-LGM valley (Figs. 3, 14D) suggest that the re-tracking of the older valley by clearing out sediment had just started when sharply stopped by descend of the rock avalanche. The instantaneous massive sediment input by rock avalanching shifted the runoff thalweg towards the West, along or near to the present one. As mentioned, along Strassberg gorge, spring limestones and talus breccias are locally present (Figs. 3, 12F). A U/Th age of 9 ± 1 ka for cement of talus breccias (Sanders et al., 2010) indicates that the bedrock level of the gorge was incised to a depth of a few meters above the present one already at that time. Taking into account the age bracket for rock avalanching (≤ 21 ka to ≥ 17.5 ka BP), this implies that the entire gorge was incised to a depth of roughly a 100 m at a mean rate of downcutting of ~12 mm/a over 8.5 ka to 9 mm/a over 11 ka; these rates are not outrageous (see Sanders et al., 2014, their Table 1). In brief, the entire Strassberg gorge was incised after the LGM and after rock avalanching, i.e, it is an epigenetic gorge.

Due to absence of Quaternary deposits or other geological markers, the development of Arzberg gorge is poorly defined. As discussed, the deglacial alluvial fan shed onto the left flank of the old Strassberg valley indicates that the Arzberg gorge either was not incised to its present depth and/or was bridged by glacial dead ice (Figs. 5, 6). The gorge follows a fault belt along the southern limit of the high-raging massif of Mt. Hohe Munde that is sculpted with deeply incised bedrock chutes (Figs. 2, 5, 6). It can be considered as certain that a similar geomorphic relation between a high-cliffed Mt.

Hohe Munde and a lower-positioned, fault-controlled precursor Arzberg valley existed also before the LGM. If the deep chutes along the SW slope of Mt. Hohe Munde (cf. Fig. 6) had continued across the present Arzberg gorge, the bedrock brinkline along the right gorge flank should show evidence for this (cf. Fig. 7). The chutes, in contrast, sharply terminate at a brinkline into Arzberg gorge; this indicates that the chutes debouched into a precursor Arzberg gorge already before the LGM. After the LGM, thus, Arzberg valley most probably became longer by headward incision, and perhaps also somewhat deeper, but did not basically change its geomorphic configuration.

8. Conclusions

(1) We had studied the proglacial to Holocene development of a catchment in the Northern Calcareous Alps. Upon proglacial sedimentation, the trunk valley (Strassberg valley) of the catchment was filled with fluvio-lacustrine deposits, before the area was overridden by ice. During deglacial ice decay, in turn, sediment shed from mountain flanks aggraded to thick talus and alluvial-fan successions. Today, some of these successions are cut off from their supply areas and are perched in isolated positions.

(2) Shortly after deglaciation, a ~11 Mm^3 rock avalanche descended, blocked Strassberg valley, and spread over and stopped on a wide plateau. A quartz OSL age of 18.77 ± 1.55 ka from loess that drapes the rock-avalanche deposit age-brackets mass wasting to between ice decay (~21–20 ka) and loess deposition.

(3) Valley blockade by the rock avalanche triggered a lateral shift of stream incision. The present Strassberg valley (1.5 km in length, down to 100 m in depth) is a post-glacial epigenetic bedrock gorge that was incised mainly during the late-glacial to early Holocene chron. The present scenery of the study area is a mosaic of landforms of highly different activity and age. Overall, the catchment is far off geomorphic equilibrium with interglacial conditions.

Acknowledgements

Financial support from grant "Nachwuchsförderung der Universität Innsbruck" (fund 2014/3/GEO-8), donated to Charlotte Gild, is gratefully acknowledged. The comments of two anonymous reviewers helped to improve the clarity of presentation.

References

Ampferer, O., 1904. Studien über die Inntalterrassen. Jahrbuch der kaiserlich-königlichen geologischen Reichsanstalt, 54, 91–160.

Ampferer, O. and Ohnesorge, T., 1912. Zirl und Nassereith. Geological map 1:75.000, 'SW.-Gruppe Nr. 28', on base of 'Topographische Spezialkarte, Zone 16, Kol IV.' Kaiserlich-königliche Geologische Reichsanstalt, Vienna.

André, M.-F., 2003. Do periglacial landscapes evolve under periglacial conditions? Geomorphology, 52, 149-164. doi:.org/10.1016/S0169-555X(02)00255-6

Auer, I., Foelsche, U., Böhm, R., Chimani, B., Haimberger, L., Kerschner, H., Koinig, K.A., Nicolussi, K. and Spötl, C. 2014. Vergangene Klimaänderungen in Österreich. In: Austrian Panel on Climate Change (APCC) (ed.), Österreichischer Sachstandsbericht Klimawandel 2014 (AAR14). Verlag der Österreichischen Akademie der Wissenschaften, Wien, pp. 227–300.

Ballantyne, C.K., 2002. Paraglacial geomorphology. Quaternary Science Reviews, 21, 1935-2017. doi. org/10.1016/S0277-379(02)00005-7

Ballantyne, C.K. and Benn, D.I., 1994. Glaciological constraints on protalus rampart development. Permafrost and Periglacial Processes, 5, 145-153.

Ballantyne, C. and Stone, J., 2013. Timing and periodicity of paraglacial rock-slope failures in the Scottish Highlands. Geomorphology, 186, 150-161. doi:10.1016/j. geomorph.2012.12.030

Ballantyne, C.K., Sandeman, G.F., Stone, J.O. and Wilson, P., 2014. Rock-slope failure following Late Pleistocene deglaciation on tectonically stable mountainous terrain. Quaternary Science Reviews, 86, 144-157. doi. org/10.1016/j.quascirev.2013.12.021

Barrett, S., Starnberger, R., Tjallingii, R., Brauer, A. and Spötl, C., 2017. The sedimentary history of the inner-alpine Inn Valley, Austria: extending the Baumkirchen type section further back in time with new drilling. Journal of Quaternary Science, 32, 63–79. https://doi. org/10.17738/ajes.2017.0004

Benn, D.I. and Owen, L.A., 2002. Himalayan glacial sedimentary environments: a framework for reconstructing and dating the former extent of glaciers in high mountains. Quaternary International, 97-98, 3-25.

Caporali, A., Neubauer, F., Ostini, L., Stangl, G. and Zuliani, D., 2013. Modelling surface GPS velocities in the Southern and Eastern Alps by finite dislocations at crustal depths. Tectonophysics, 590, 136–150. https://dx.doi. org/10.1016/j.tecto.2013.01.016

Church, M. and Ryder, J.M., 1972. Paraglacial sedimentation: a consideration of fluvial processes conditioned by glaciation. Geological Society of America Bulletin, 83, 3059-3071.

Collins, G.S. and Melosh, H.J., 2003. Acoustic fluidization and the extraordinary mobility of sturzstroms. Journal of Geophysical Research, 108, B10, 2473. https://doi. org/10.1029/2003JB002465.

Cossart, E., Braucher, R., Fort, M., Bourlés, D.L. and Carcaillet, J., 2008. Slope instability in relation to glacial debuttressing in alpine areas (Upper Durance catchment, southeastern France): Evidence from field data and ^{10}Be cosmic ray exposure ages. Geomorphology, 95, 3-26. doi:10.1016/j.geomorph.2006.12.022

Crosta, G. B., Chen, H. and Lee, C.F., 2004. Replay of the 1987 Val Pola Landslide, Italian Alps. Geomorphology, 60, 127–146. https://doi.org/10.1016/j. geomorph.2003.07.015

Cruden, D.M. and Hungr, O., 1986. The debris of the Frank Slide and theories of rock-avalanche mobility. Canadian Journal of Earth Sciences, 23, 425–432.

Curry, A.M. and Ballantyne, C.K., 1999. Paraglacial modification of glacigenic sediment. Geografiska Annaler, 81A, 409-419.

Curry, A.M., Cleasby, V. and Zukowskyj, P., 2006. Paraglacial response of steep, sediment-mantled slopes to post-'Little Ice Age' glacier recession in the central Swiss Alps. Journal of Quaternary Science, 21, 211–225. doi: 10.1002/jqs.954

Davies, T.R. and McSaveney, M.J., 2002. Dynamic simulation of the motion of fragmenting rock avalanches. Canadian Geotechnical Journal, 39, 789–798. https://doi.org/10.1139/T02-035

Davies, T.R. and McSaveney, M.J., 2009. The role of rock fragmentation in the motion of large landslides. Engineering Geology, 109, 67–79. https://doi.org/10.1016/j.enggeo.2008.11.004

De Blasio, F.V. and Crosta, G.B., 2014. Simple physical model for the fragmentation of rock avalanches. Acta Mechanica, 225, 243–252. https://doi.org/10.1007/s00707-013-0942-y

Dufresne, A. and Davies, T.R., 2009. Longitudinal ridges in mass movement deposits. Geomorphology, 105, 171–181. https://doi.org/10.1016/j.geomorph.2008.09.009

Dufresne, A., Prager, C. and Bösmeier, A., 2015. Insights into rock avalanche emplacement processes from detailed morpho-lithological studies of the Tschirgant deposit (Tyrol, Austria). Earth Surface Processes and Landforms, 41, 587–602. doi: 10.1002/esp.3847

Erismann, T. H. and Abele, G., 2001. Dynamics of rockslides and rockfalls. Springer (Berlin), 316 pp.

Evans, S. G., Scarascia Mugnozza, G., Strom, A. l., Hermanns, R. L., Ischuk, A., Vinnichenko, S., 2006. Landslides from massive rock slope failure and associated phenomena. In: S.G. Evans, G. Scarascia Mugnozza, A. Strom and R.L. Hermanns (eds.), Landslides from massive rock slope failure. NATO Science Series, Springer, Dordrecht, pp. 3–52.

French, H. and Harbor, J., 2013. The development and history of glacial and periglacial geomorphology. In: Shroder, J. (Editor in Chief), Giardino, R., Harbor, J. (Eds.), Treatise on Geomorphology. Academic Press, San Diego, CA, volume 8, Glacial and Periglacial Geomorphology, pp. 1–18. http://dx.doi.org/10.1016/B978-0-12-374739-6.00190-1

Frisch, W., Székely, B., Kuhlemann, J. and Dunkl, I., 2000. Geomorphological evolution of the Eastern Alps in response to Miocene tectonics. Zeitschrift für Geomorphologie, Neue Folge, 44, 103–138.

Fügenschuh, B., Seward, D. and Mancktelow, N., 1997. Exhumation in a convergent orogen: the western Tauern window. Terra Nova, 9, 213–217.

Fügenschuh, B., Mancktelow, N.S. and Schmid, S.S., 2012. Comment on Rosenberg and Garcia: Estimating displacement along the Brenner Fault and orogen-parallel extension in the Eastern Alps, Int J Earth Sci (Geol Rundsch) (2011) 100: 1129–1145. International Journal of Earth Sciences, 101, 1451–1455. https://doi.org/10.1007/s00531-011-0725-4

Geyh, M.A., 2005. Handbuch der physikalischen und chemischen Altersbestimmung. Wissenschaftliche Buchgesellschaft, Darmstadt, 211 pp.

Gild, C., Geitner, C. and Sanders, D., 2018. Discovery of a landscape-wide drape of late-glacial aeolian silt in the western Northern Calcareous Alps (Austria): First results and implications. Geomorphology, 301, 39–52. https://doi.org/10.1016/j.geomorph.2017.10.025

Handy, M.R., Ustaszewski, K. and Kissling, E., 2015. Reconstructing th Alps-Carpathians–Dinarides as a key to understanding switches in subduction polarity, slab gaps and surface motion. International Journal of Earth Sciences, 104, 1–26. https://doi.org/10.1007/s00531-014-1060-3

Heck, F.R. and Speed, R.C., 1987. Triassic olistostrome and shelf-basin transition in the western Great Basin: Paleogeographic implications. Geological Society of America Bulletin, 99, 539–551.

Herbst, P., Hilberg, S., Draxler, I., Zauner, H. and Riepler, F., 2009. The facies and hydrogeology of an inneralpine Pleistocene terrace based on in integrated study – deep well Telfs. Austrian Journal of Earth Sciences, 102/2, 149–156.

Hewitt, K., 1998. Catastrophic landslides and their effects on the Upper Indus streams, Karakoram Himalaya, northern Pakistan. Geomorphology, 26, 47–80.

Hungr, O., Evans, S.G., Bovis, M.J. and Hutchinson, J.N., 2001. A review of the classification of landslides of flow type. Environmental and Engineering Geoscience, VII/3, 221–238.

Hungr, O., Leroueil, S. and Picarelli, L., 2012. Varnes classification of landslide types, an update. In: E. Eberhardt, C. Froese, A.K. Turner and S. Leroueil (eds.), Landslides and Engineered Slopes: Protecting Society through Improved Understanding. CRC Press/Balkema, Taylor and Francis Group, London, pp. 47–58.

Jibson, R.W., 2013. Mass-movement causes: earthquakes. In: J. Shroder (Editor in Chief), R.A. Marston and M. Stoffel (eds.), Treatise on Geomorphology. Academic Press, San Diego, CA, vol. 7, Mountain and Hillslope Geomorphology, pp. 223–229.

Jiskoot, H., 2011. Long-runout rockslide on glacier at Tsar Mountain, Canadian Rocky Mountains: potential triggers, seismic and glaciological implications. Earth Surface Processes and Landforms, 36, 203–216. https://doi.org/10.1002.esp.2039

Kampf, S.K. and Mirus, B.B., 2013. Subsurface and surface flow leading to channel initiation. In: Shroder, J. (Editor in Chief) and Wohl, E. (Ed.), Treatise on Geomorphology. Academic Press, San Diego, CA, vol. 9, Fluvial Geomorphology, pp. 22–42.

Keefer, D.K., 2013. Landslides generated by earthquakes: immediate and long-term effects. In: Shroder, J. (Editor in Chief) and Owen, L.A. (Ed.), Treatise on Geomorphology. Academic Press, San Diego, CA, vol. 5, Tectonic Geomorphology, pp. 250–266.

Kellerer-Pirklbauer, A., Proske, H. and Strasser, V., 2010. Paraglacial slope adujustment since the end of the Last Glacial Maximum and its long-lasting effect on secondary mass-wasting processes: Hauser Kaibling, Austria. Geomorphology, 120, 65-76. doi.org/10.1016/j.geomorph.2009.09.016

Korup, O. and Tweed, F., 2007. Ice, moraine, and landslide dams in mountainous terrain. Quaternary Science Reviews, 26, 3406–3422. https://doi.org/10.1016/j.quascirev.2007.10.012

Lenhardt, W.A., 2007. Earthquake-triggered landslides in Austria – Dobratsch revisited. Jahrbuch der Geologischen Bundesanstalt, 147, 193–199.

Lenhardt, W.A., Freudenthaler, C., Lippitsch, R. and Fiegweil, E., 2007. Focal-depth distributions in the Austrian Eastern Alps based on macroseismic data. Austrian Journal of Earth Sciences, 100, 66–79.

Linzer, H.-G., Ratschbacher, L. and Frisch, W., 1995. Transpressional collision structures in the upper crust: the fold-thrust belt of the Northern Calcareous Alps. In: F. Neubauer and E. Wallbrecher (eds.), Tectonics of the Alpine-Carpathian-Pannonian Region. Tectonophysics, 242, 41–61.

Linzer, H.-G., Moser, F., Nemes, F., Ratschbacher, L. and Sperner, B., 1997. Build-up and dismembering of the eastern Northern Calcareous Alps. Tectonophysics, 272, 97–124.

Linzer, H.-G., Decker, K., Peresson, H., Dell'Mour, R. and Frisch, W., 2002. Balancing lateral orogenic float of the Eastern Alps. Tectonophysics, 354, 211–237.

Locat, P., Couture, R., Leroueil, S., Locat, J. and Jaboyedoff, M., 2006. Fragmentation energy in rock avalanches. Canadian Geotechnical Journal, 43, 830–851. https://doi.org/10.1139/T06-045

Nasir, A., Lenhardt, W., Hintersberger, E. and Dicker, K., 2013. Assessing the completeness and instrumental earthquake data in Austria and the surrounding areas. Austrian Journal of Earth Sciences, 106/1, 90–102.

Niederstrasser, L., 2017. Zusammensetzung und Kartierung einer Lage von siliziklastischem Silt in einer Schuttfächer-Abfolge (Mieminger Plateau, Nördliche Kalkalpen). Bachelor thesis, University of Innsbruck, 43 pp.

Machatschek, F., 1933. Tal- und Glazialstudien im oberen Inngebiet. Mitteilungen der Geographischen Gesellschaft in Wien, 76, 5–52.

Mandl, G.W., 2000. The Alpine sector of the Tethyan shelf - Example of Triassic to Jurassic sedimentation and deformation from the Northern Calcareous Alps. Mitteilungen der Österreichischen Geologischen Gesellschaft, 92, 61–77.

McSaveney, M.J. and Davies, T.R.H., 2002. Rapid rock-mass flow with dynamic fragmentation: Inferences from the morphology and internal structure of rockslides and rock avalanches. In: S.G. Evans, G. Scarascia Mugnozza, A. Strom and R.L. Hermanns (eds.), Landslides from massive rock slope failure. NATO Science Series, Springer, Dordrecht, pp. 285–304.

McSaveney, M.J. and Davies, T.R., 2009. Surface energy is not one of the energy losses in rock comminution. Engineering Geology, 109, 109–113. https://doi.org/10.1016/j.enggeo.2008.11.001

Meigs, A., Krugh, W.C., Davis, K., Bank, G., 2006. Ultra-rapid landscape response and sediment yield following glacier retreat, Ice Bay, southern Alaska. Geomorphology, 78, 207-221. doi:10.1016/j.geomorph.2006.01-029

Montgomery, D.R. and Buffington, J.M., 1997. Channel-reach morphology in mountain drainage basins. Geological Society of America Bulletin, 109, 596–611.

Moran, A.P., Ivy-Ochs, S., Vockenhuber, C. and Kerschner, H., 2016. First ^{36}Cl exposure ages from a moraine in the Northern Calcareous Alps. E&G Quaternary Science Journal, 65, 145–155. https://doi.org/10.3285/eg.65.2.03

Mutschlechner, G., 1948. Spuren des Inngletschers im Bereich des Karwendelgebirges. Jahrbuch der Geologischen Bundesanstalt, 3–4, 155–206.

Ortner, H., Reiter, F. and Brandner, R., 2006. Kinematics of the Inntal shear zone–sub-Tauern ramp fault system and the interpretation of the TRANSALP seismic section, Eastern Alps, Austria. Tectonophysics, 414, 241–258. https://doi.org/10.1016/j.tecto.2005.10.017

Orwin, J.F. and Smart, C.C., 2004. The evidence for paraglacial sedimentation and its temporal scale in the deglacierizing basin of Small River Glacier, Canada. Geomorphology, 58, 175-202. doi.org/10.1016/j.geomorph.2003.07.005

Ostermann, M., Sanders, D. and Kramers, J., 2006. ^{230}Th/^{234}U ages of calcite cements of the proglacial valley fills of Gamperdona and Bürs (Riss ice age, Vorarlberg, Austria): geological implications. Austrian Journal of Earth Sciences, 99, 31–41.

Ostermann, M. and Sanders, D., 2012. Post-glacial rockslides in a 200x130 km area of the Alps: Characteristics, ages, and uncertainties. In: E. Eberhardt, C. Froese, A.K. Turner and S. Leroueil (eds.), Landslides and Engineered Slopes: Protecting Society through Improved Understanding. CRC Press/Balkema, Taylor and Francis Group, London, vol. 1, 659–663.

Ostermann, M. and Sanders, D., 2016. The Brenner pass rock avalanche cluster suggests a close relation between long-term slope deformation (DSGSDs and translational rock slides) and catastrophic failure. Geomorphology, 289, 44–59. https://doi.org/10.1016/j.geomorph.2016.12.018

Ostermann, M., Ivy-Ochs, S., Sanders, D. and Prager, C., 2016. Multi-method (^{14}C, ^{36}Cl, ^{234}U/^{230}Th) age bracketing of the Tschirgant rock avalanche (Eastern Alps): Implications for absolute dating of catastrophic mass–wasting. Earth Surface Processes and Landforms 42, 1110–1118. https://doi.org/10.1002/esp.4077

Penck, A. and Brückner, E., 1909. Die Alpen im Eiszeitalter. Tauchnitz, Leipzig, 1199 pp.

Perinotto, H., Schneider, J.-L., Bachèlery, P., Le Bourdonnec, F.-X., Famin, V. and Michon, L., 2015. The extreme mobility of debris avalanches: A new model

of transport mechanism. Journal of Geophysical Research: Solid Earth, 120, 8110–8119. https://doi.org/10-1102/2015JB011994

Pirulli, M., 2009. The Thurwieser rock avalanche (Italian Alps): Description and dynamic analysis. Engineering Geology, 109, 80–92. https://doi.org/10.1016/j.enggeo.2008.10.007

Pollet, N. and Schneider, J.-L.M., 2004. Dynamic disintegration processes accompanying transport of the Holocene Flims sturzstrom (Swiss Alps). Earth and Planetary Science Letters, 221, 433–448. https://doi.org/10.1016/S0012-821X/(04)00071-8

Poscher, G., 1993. Neuergebnisse der Quartärforschung in Tirol. In: Hauser, C. and Nowotny, A. (coord.), Geologie der Oberinntaler Raumes, Schwerpunkt Blatt 144 Landeck. Arbeitstagung der Geologischen Bundesanstalt, 7–27.

Poschinger, A. von and Kippel, T., 2009. Alluvial deposits liquefied by the Flims rockslide. Geomorphology, 103, 50–56. https://doi.org/10.1016/j.geomorph.2007.09.016

Prager, C., Zangerl, C., Patzelt, G. and Brandner, R., 2008. Age distribution of fossil landslides in the Tyrol (Austria) and its surrounding areas. Natural Hazards and Earth System Science, 8, 377–407. https://doi.org/10.5194/nhess-8-3772008, 2008

Preh, A. and Sausgruber, J.T., 2015. The extraordinary rock-snow avalanche of Alpl, Tyrol, Austria. Is it possible to predict the runout by means of single-phase Voellmy-or Coulomb-type models? In: G. Lollino, D. Giordan, G.B. Crosta, J. Corominas, R. Azzam, J. Wasowski and N. Sciarra(eds.), Engineering Geology for Society and Territory–Volume 2: Landslide Processes. Springer International Publishing, Cham, Switzerland, pp. 1907–1911.

Ratschbacher, L., Frisch, W., Linzer, H.-G. and Merle, O., 1991. Lateral extrusion in the eastern Alps, Part 2: Structural analysis. Tectonics, 10, 257–271.

Ravazzi, C., Badino, F., Marsetti, D., Patera, G. and Reimer, P.J., 2012. Glacial to paraglacial history and forest recovery in the Oglio glacier system (Italian Alps) between 26 and 15 ka cal BP. Quaternary Science Reviews, 58, 146-161. doi.org/10.1016/j.quatscirev.2012.10.017

Reinecker, J. and Lenhardt, W.A., 1999. Present-day stress field and deformation in eastern Austria. International Journal of Earth Sciences, 88, 532–550.

Reiter, F., 2017. Active seismotectonic deformation north of the Dolomites Indenter, Eastern Alps. PhD thesis, University of Innsbruck, 254 pp.

Reiter, F., Lenhardt, W.A. and Brandner, R., 2005. Indications for activity of the Brenner normal fault zone (Tyrol, Austria) from seismological and GPS data. Austrian Journal of Earth Sciences, 97, 16–23.

Reitner, J.M., 2007. Glacial dynamics at the beginning of Termination I in the Eastern Alps and their stratigraphic implications. Quaternary International,164–165, 64–84. https://doi.org/10.1016/j.quaint.2006-12.016

Reitner, J. M., Ivy-Ochs, S., Drescher-Schneider, R., Hajdas, I. and Linner, M., 2016. Reconsidering the current stratigraphy of the Alpine Lateglacial: Implications of the sedimentary and morphological record of the Lienz area (Tyrol/Austria). E&G Quaternary Science Journal, 65, 113-144. doi:10.3285/eg.65.2.02

Sanders, D., 2012. Effects of deglacial sedimentation pulse, followed by incision: A case study from a catchment in the Northern Calcareous Alps (Austria). E&G Quaternary Science Journal, 61, 16–31. https://doi.org/10.3285/eg.61.1.02

Sanders, D., Ostermann, M. and Kramers, J., 2009. Quaternary carbonate-rocky talus slope successions (Eastern Alps, Austria): sedimentary facies and facies architecture. Facies, 55, 345–373. https://doi.org/10.1007/s10347-008-0175-z

Sanders, D., Ostermann, M. and Kramers, J., 2010. Meteoric diagenesis of Quaternary carbonate-rocky talus slope successions (Northern Calcareous Alps, Austria). Facies, 56, 27–46. https://doi.org/10.1007/s10347-009-0194-4

Sanders, D., Ostermann, M., Brandner, R. and Prager, C., 2010. Meteoric lithification of catastrophic rockslide deposits: diagenesis and significance. Sedimentary Geology, 223, 150–161. https://doi.org/10.1016/j.sedgeo.2009.11.007

Sanders, D. and Ostermann, M., 2011. Post-last glacial alluvial fan and talus slope associations (Northern Calcareous Alps, Austria): A proxy for Late Pleistocene to Holocene climate change. Geomorphology, 131, 85–97. https://doi.org/10.1016/j.geomorph.2011.04.029

Sanders, D., Widera, L. and Ostermann, M., 2014. Two-layer scree/snow-avalanche triggered by rockfall (Eastern Alps): significance for sedimentology of scree slopes. Sedimentology, 61, 996–1030. https://doi.org/10.1111/sed.12083

Sanders, D., Preh, A., Sausgruber, T., Pomella, H., Ostermann, M. and Sedlmaier, A., 2016. Rockfall-triggered, long-runout two-layer scree/snow avalanche, old rock avalanche deposit, and epigenetic canyon incision (Northern Calcareous Alps): consequences for hazard assessment and landscape history. Geo.Alp, 13, 183–202.

Sanders, D., Preh, A. and Sausgruber, T., 2016. Long-runout rock/snow flows: an underrated type of mountain hazard. In: Ortner, H. (ed.), GeoTirol2016, Annual Meeting of DGGV and PANGEO Austria, Abstract Volume, p. 295.

Sanders, D., Ortner, H. and Pomella, H., 2018. Stratigraphy and deformation of Pleistocene talus in relation to a normal fault zone (central Apennines, Italy). Sedimentary Geology, 373, 77-97. https://doi.org/10.1016/j.sedgeo.2018.05.013

Schmid, S. M., Fügenschuh, B., Kissling, E. and Schuster, R., 2004. Tectonic map and overall architecture of the Alpine orogen. Eclogae Geologicae Helvetiae, 97, 93–117. https://doi.org/10.1007/s00015-004-1113-x

Schneider, J.F., Gruber, F.E. and Mergili, M., 2011. Recent cases and geomorphic evidence of landslide-dammed lakes and related hazard in the mountains of Central Asia. In: Proceedings of the Second World Landslide Forum, 3-11 October 2011, Rome, 6 pp.

Schrott, L., Hufschmidt, G., Hankammer, M., Hoffmann, T. and Dikau, R., 2004. Spatial distribution of sediment storage types and quantification of valley fill deposits in an alpine basin, Reintal, Bavarian Alps, Germany. Geomorphology, 55, 45-63. doi.org/10.1016/S0169-555X(03)00131-4

Senarclens-Grancy, W., 1938. Stadiale Moränen in der Mieminger Kette und im Wetterstein. Jahrbuch der Geologischen Bundesanstalt, 88, 1–12.

Severinghaus, J.P., Sowers, T., Brook, E.J., Alley, R.B. and Bender, M.L., 1998. Timing of abrupt climate change at the end of the Younger Dryas interval from thermally fractionated gases in polar ice. Nature, 391, 141–148.

Shugar, D.H. and Clague, J.J., 2011. The sedimentology and geomorphology of rock avalanche deposits on glaciers. Sedimentology, 58, 1762-1783. https.//doi.org/10.1111/j.1365-3091.2011.01238.x

Sundell, K.A. and Fisher, R.V., 1985. Very coarse grained fragmental rocks: A proposed size classification. Geology, 13, 692–695.

Tollmann, A., 1976. Analyse des klassischen nordalpinen Mesozoikums. Franz Deuticke, Vienna, 580 pp.

Tunnicliffe, J.F. and Church, M., 2011. Scale variation of post-glacial sediment yield in Chilliwack valley, British Columbia. Earth Surface Processes and Landforms, 36, 229-243. doi:10.1002/esp.2093

Van Husen, D., 1983. A model of valley bottom sedimentation during climatic changes in a humid alpine environment. In: E.B. Evenson, C. Schlüchter and J. Rabassa (eds.), Tills and Related Deposits. A.A. Balkema, Rotterdam, pp. 341–344.

Van Husen, D., 1987. Die Ostalpen in den Eiszeiten. Populärwissenschaftliche Veröffentlichungen der Geologischen Bundesanstalt, Geologische Bundesanstalt, Wien. Ferdinand Berger and Söhne GmbH, Horn, 24 pp., 1 map.

Van Husen, D. and Reitner, J., 2011. An outline of the Quaternary stratigraphy of Austria. E&G Quaternary Science Journal, 60, 366–387. https://doi.org/10.3285/eg.60.2-3.09

Wang, X. and Neubauer, F., 1998. Orogen-parallel strike-slip faults bordering metamorphic core complexes: the Salzach-Enns fault zone in the Eastern Alps, Austria. Journal of Structural Geology, 20, 799–818.

Westreicher, F., Kerschner, H., Nicolussi, K., Ivy-Ochs, S. and Prager, C., 2014. Ein Bergsturz am Mieminger Plateau oder wie aus einer "postglazialen Moräne" ein holozäner Bergsturz wurde. In: K.A. Koinig, R. Starnberger and C. Spötl (eds.), Deuqua 2014, 37: Hauptversammlung der deutschen Quartärvereinigung, Innsbruck 2014. Innsbruck University Press, Conference Series, Universität Innsbruck, pp. 149–150.

Wölfler, A., Kurz, W., Fritz, H. and Stüwe, K., 2011. Lateral extrusion in the Eastern Alps revisited: Refining the model by thermochronological, sedimentary, and seismic data. Tectonics, 30, TC4006, doi:10.1029/2010TC002782, 2011.

Submitted: 13 03 2018
Accepted: 01 10 2018

Diethard SANDERS[1)*)], Hannah POMELLA[1)] & Charlotte GILD[2)]

[1)] Institute of Geology, University of Innsbruck, A-6020 Innsbruck, Austria;

[2)] Institute of Geography, University of Innsbruck, A-6020 Innsbruck, Austria;

[*)] Corresponding author: Diethard.G.Sanders@uibk.ac.at